

Traffic-Rule-Compliant Trajectory Repair via Satisfiability Modulo Theories and Reachability Analysis

Yuanfei Lin, Zekun Xing, Xuyuan Han, and Matthias Althoff

Abstract—Complying with traffic rules is challenging for automated vehicles, as numerous rules need to be considered simultaneously. If a planned trajectory violates traffic rules, it is common to replan a new trajectory from scratch. We instead propose a trajectory repair technique to save computation time. By coupling satisfiability modulo theories with set-based reachability analysis, we determine if and in what manner the initial trajectory can be repaired. Experiments in high-fidelity simulators and in the real world demonstrate the benefits of our proposed approach in various scenarios. Even in complex environments with intricate rules, we efficiently and reliably repair rule-violating trajectories, enabling automated vehicles to swiftly resume legally safe operation in real-time.

Index Terms—Motion and path planning, formal methods in robotics and automation, intelligent transportation systems, trajectory repair.

I. INTRODUCTION

JUST like human drivers, automated vehicles must explicitly comply with traffic rules to ensure their safe operation on roads. If this is done carefully, automated driving can gain the necessary public trust, and responsible operators can mitigate potential liability claims in case of accidents. However, despite the paramount importance of rule compliance, existing motion planning algorithms, as highlighted in recent surveys [1]–[4], either overlook traffic rules, incorporate them implicitly using deep learning approaches [5], or address only a limited selection [6], [7].

Runtime verification (aka *monitoring*) is an efficient method to verify if the planned trajectory aligns with expected behaviors [8]–[10]. If planned trajectories are monitored and identified as rule-violating, it is common to replan them within a receding-horizon planning framework. Nevertheless, replanning the entire trajectory is often undesired and inefficient for several reasons:

- 1) it relies on the strong assumption that the used planner inherently accommodates every traffic rule;
- 2) replanning typically requires substantially more computational resources than focusing on adjusting specific trajectory segments; and
- 3) frequent replanning can lead to unpredictable and inconsistent behavior, potentially causing confusion among other traffic participants [11, Sec. I].

Manuscript received Month Date, Year; revised Month Date, Year.

The authors are with the Department of Computer Engineering, Technical University of Munich, 85748 Garching, Germany.

{yuanfei.lin, zekun.xing, xuyuan.han, althoff}@tum.de (Corresponding author: Yuanfei Lin.)

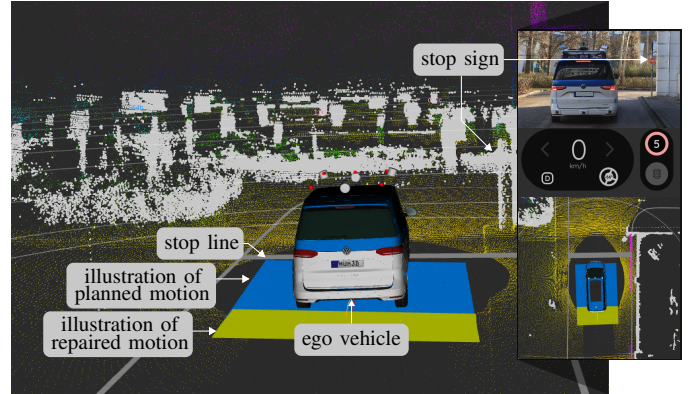


Fig. 1: Snapshot from our real-world driving experiments. Our trajectory repair approach dynamically adjusts planned trajectories that violate traffic rules in real time. For example, it enforces the stop line rule by requiring the vehicle to halt before the marked line for the specified duration. The motion plans are illustrated by widening the path to be followed for improved visibility and are referenced from the rear axle. The animations of the experiments are available at <https://commonroad.github.io/repair-to-drive/>.

Therefore, we propose a trajectory repair framework that selectively refines a planned trajectory to address violations of traffic rules (see Fig. 1).

A. Literature Overview

We categorize existing works on rule-informed motion planning, trajectory replanning, and repair techniques for automated vehicles. Since our work focuses on traffic rules derived from legal resources and consultations with lawyers, we do not review works on modifying specifications online [12]–[14].

1) *Rule-Informed Motion Planning*: Traffic rules are initially described in natural language, which usually introduces ambiguity and unintended interpretations. Formal methods address this issue by using rigorous mathematical formalization [4]. In particular, temporal logic is extensively used to formalize safety requirements and complex traffic rules. Examples include linear temporal logic (LTL) [15], [16], metric temporal logic (MTL) [17]–[19], signal temporal logic (STL) [20], and their variants [21], [22].

Several studies integrate LTL specifications into the motion planning problem by formulating them as automata and use rapidly-exploring random trees (RRTs) [23] to plan trajectories [24]–[26]. The automata-based approaches are computationally expensive, and the RRT algorithm is only probabilistically complete [27]. In contrast, MTL and STL have the advantage of quantitatively evaluating the degree of satisfaction or vi-

olation using robustness (aka *robustness degree*) [28], [29]. Thus, we can maximize the level of satisfaction by encoding the MTL and STL formulas as mixed-integer constraints and including the robustness in the cost function of optimization-based planners [30]. But this approach scales poorly with an increasing number of integer variables. Recent efforts leverage neural-network-based methods or control barrier functions to generate trajectories satisfying STL tasks with high computational efficiency [31]–[33]. However, they cannot easily consider complex specifications due to their assumptions, such as the existence of valid control barrier functions [31], [32]. In addition, the authors of [34]–[36] propose using reachability analysis and model checking to prune the search space of motion planners.

2) *Trajectory Replanning*: In classical motion planning, incremental techniques are widely employed to replan trajectories by dynamically adapting the motion planner to changing environments [2]. Search algorithms such as lifelong planning A* [37], [38], D* [39], and anytime repairing A* [40] are incremental variants of the original A* algorithm. Similarly, many sampling-based motion planners [41]–[45] use incremental strategies to progressively explore the solution space. In task planning with LTL specifications, several studies [46]–[48] promote an incremental method for mending the product automaton, which combines an abstract model of the system and the specification automaton. To ensure the safety of black-box motion planners, the authors of [49] use reachability analysis to verify safety and replan unsafe trajectories by sampling from feasible configuration spaces. Likewise, the approach proposed in [50] replans actions suggested by a reinforcement learning agent when they violate traffic rules. Furthermore, the work presented in [51] harnesses the power of large language models to enhance the performance of motion planners. However, these methods are tightly integrated within the motion planner, which limits their flexibility.

3) *Trajectory Repair*: Trajectory repair differs from replanning by relying solely on the output of the motion planner, either by making local adjustments or branching off.

a) *Local Trajectory Repair*: Local trajectory repair typically uses the planned trajectory as a reference to improve its quality when it fails to meet the given criteria. For example, the authors of [52] employ an optimization procedure that incorporates trajectory smoothness as an additional constraint. A similar regime is outlined in [53]–[59], where search algorithms, optimizers, or parametric curves are used to repair the initial plan. In addition, the initial trajectory can be locally deformed to avoid collisions, either by modeling it as an elastic band [60] or through an affine transformation [61]. However, when addressing the nonholonomic motion of a vehicle, solving the two-point boundary value problem – finding a trajectory that satisfies given initial and final conditions – poses significant challenges, especially in real-time applications.

b) *Branching Off From Trajectories*: When the initially planned result maintains a sufficiently high quality, it can be partially reused and a new partial trajectory can be branched off to meet all requirements. The works in [62]–[68] bear conceptual similarities to our approach in this regard. They

account for potential future scenario evolutions, resulting in trajectories branching off for each alternative future scenario. Notably, the authors of [66] highlight the benefits of delaying branching points as much as possible, which reduces the number of constraints in the trajectory optimization problem and leaves more reaction time for the vehicle to handle potential hazards. This also aligns with the preference of system designers for safety systems to intervene at the latest possible point in time [69]. However, their selection of branching points is not suitable for rule-compliant trajectory repair, as these are either defined solely by divergences in future predictions [66], determined through a static choice [63], [64], or lack well-defined frameworks [62], [68]. To address these limitations, we proposed using criticality measures in our previous work [70]–[72], as they objectively assess behavioral safety and offer a systematic approach for determining the appropriate timing of interventions. To efficiently obtain a satisfactory solution, satisfiability modulo theories (SMT) [73] is used to determine whether and how the violated rules can be satisfied.

B. Contributions and Outline

Building upon our previous work [70]–[72], we present a trajectory repair approach to promote compliance with formalized traffic rules of an automated vehicle, referred to as the *ego vehicle* from now on. In particular, unlike our previous work, our approach simultaneously:

- 1) supports traffic rules formalized in STL with arbitrary temporal operators;
- 2) employs for the first time model predictive robustness as enhanced heuristics for Boolean satisfiability (SAT) solving – an NP-complete problem – within an SMT solver. This also makes it possible to obtain reasonable robustness values without excessive manual tuning;
- 3) for the first time, applies set-based reachability analysis to compute the spatio-temporal constraints needed to repair trajectories;
- 4) requires less computation time in more critical scenarios with smaller solution spaces;
- 5) can be applied to arbitrary traffic scenarios, covering diverse driving environments, such as interstates and intersections; and
- 6) has been extensively validated through both open-loop and closed-loop traffic simulations, as well as real-world testing on a research vehicle, with each validation type using a different nominal planner.

This article is structured as follows: After introducing the preliminaries and problem statement in Sec. II, we present an overview of our approach in Sec. III. The abstraction process for propositional rule formulas is described in Sec. IV, followed by SAT solving and trajectory repair in Sec. V and Sec. VI, respectively. Finally, we evaluate our concept in Sec. VII before drawing conclusions in Sec. VIII.

II. PRELIMINARIES AND PROBLEM STATEMENT

A. System Description and Notations

An index $k \in \mathbb{N}_0$ corresponds to a discrete time step $t_k = k\Delta t$, where $\Delta t \in \mathbb{R}_+$ is a fixed time increment. The motion

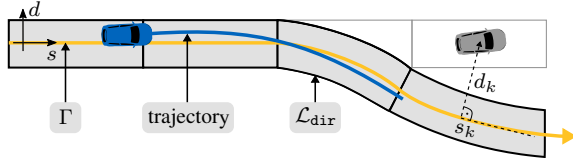


Fig. 2: Vehicle localization in the curvilinear coordinate system defined with respect to the reference path Γ , which corresponds to the centerline of \mathcal{L}_{dir} .

of vehicles is modeled as a discrete-time system:

$$\mathbf{x}_{k+1} = f(\mathbf{x}_k, \mathbf{u}_k), \quad (1)$$

where $\mathbf{x}_k \in \mathbb{R}^{n_x}$ is the state vector and $\mathbf{u}_k \in \mathbb{R}^{n_u}$ is the input vector. The state and input are bounded by sets of admissible values: $\forall k \in [0, h]: \mathbf{x}_k \in \mathcal{X}_k$ and $\forall k \in [0, h-1]: \mathbf{u}_k \in \mathcal{U}_k$, where $h \in \mathbb{N}_+$ is the final time step. We denote the solution of (1) at time step k as $\chi(k, \mathbf{x}_0, \mathbf{u}_{[0, k-1]})$, given an initial state \mathbf{x}_0 and an input trajectory $\mathbf{u}_{[0, k-1]}$ for the time interval $[0, k-1]$. For simplicity, we sometimes write χ instead of $\chi([0, h], \mathbf{x}_0, \mathbf{u}_{[0, h-1]})$. The road network \mathcal{L} is composed of a set of lanelets [74], each defined by polylines that establish its left and right boundaries. Given a planned or predicted trajectory, we compute a reference path Γ [75], which uniquely corresponds to a sequence of lanelets $\mathcal{L}_{\text{dir}} \subset \mathcal{L}$ aligned with the driving direction. As depicted in Fig. 2, a curvilinear coordinate system is derived from Γ for locating the vehicle using its longitudinal position s and lateral deviation d from Γ at s [75]. Let \square represent a variable. The initial and repaired values of \square are denoted by \square^{ini} and \square^{rep} , respectively. Values associated with the ego vehicle are represented by \square_{ego} , and those associated with an obstacle $\text{obs} \in \mathcal{B}$ by \square_{obs} , where \mathcal{B} denotes the set of rule-relevant obstacles. The concatenated states of vehicles is denoted by $\omega_k := [\mathbf{x}_{\text{ego}, k}^T, \mathbf{x}_{\text{obs}_0, k}^T, \dots, \mathbf{x}_{\text{obs}_{|\mathcal{B}|-1}, k}^T]^T \in \mathcal{X}_k^{|\mathcal{B}|+1}$.

B. Signal Temporal Logic

For traffic rule evaluation, we consider a discrete-time signal $\omega := \omega_0, \dots, \omega_k, \dots, \omega_h$. Given formulas φ , φ_1 , and φ_2 , the syntax of STL is defined as [76, Sec. 2.1]:

$$\varphi := p \mid \neg\varphi \mid \varphi_1 \vee \varphi_2 \mid \varphi_1 \mathbf{S}_{[a, b]} \varphi_2 \mid \varphi_1 \mathbf{U}_{[a, b]} \varphi_2, \quad (2)$$

where $p := \alpha(\omega_k) > 0$ is an atomic predicate, with $\alpha: \mathcal{X}_k^{|\mathcal{B}|+1} \rightarrow \mathbb{R}$. The symbols \neg and \vee denote Boolean *negation* and *disjunction* operators. Additionally, $\varphi_1 \mathbf{S}_{[a, b]} \varphi_2$ and $\varphi_1 \mathbf{U}_{[a, b]} \varphi_2$ represent the temporal *since* and *until* operators, respectively, with a time bound of $[a, b]$, where $a, b \in \mathbb{N}_0$ and $b \geq a$. The logical *True* and *False* are denoted as \top and \perp , respectively, and the valuation of a formula φ is denoted as $\llbracket \varphi \rrbracket$, e.g., $\llbracket \varphi \rrbracket = \top$. To simplify notation, we omit the interval from temporal operators when it extends to the end of the input signal, which is always finite in this work. If a signal ω complies with φ at time step k , we write $\omega_k \models \varphi$. If not, we write $\omega_k \not\models \varphi$. Additional temporal logic operators can be constructed from (2) (see [76, Sec. 2.1]), such as $\varphi_1 \wedge \varphi_2 := \neg(\neg\varphi_1 \vee \neg\varphi_2)$ (*conjunction*), $\varphi_1 \Rightarrow \varphi_2 := \neg\varphi_1 \vee \varphi_2$ (*implication*), $\mathbf{P}\varphi := \perp \mathbf{S}\varphi$ (*previous*), $\mathbf{O}_{[a, b]}\varphi := \top \mathbf{S}_{[a, b]}\varphi$ (*once*), $\mathbf{F}_{[a, b]}\varphi := \top \mathbf{U}_{[a, b]}\varphi$ (*eventually*), $\mathbf{H}_{[a, b]}\varphi := \neg \mathbf{O}_{[a, b]}\neg\varphi$ (*historically*), and $\mathbf{G}_{[a, b]}\varphi := \neg \mathbf{F}_{[a, b]}\neg\varphi$ (*globally*).

In this article, we focus on future-time temporal operators as the outermost operators, specifically \mathbf{F} and \mathbf{G} , which are most frequently used in motion planning. The past-time operators \mathbf{O} and \mathbf{H} can be defined analogously, as they mirror their future-time counterparts \mathbf{F} and \mathbf{G} , respectively, operating in reverse time. We now define the robustness of STL formulas.

Definition 1 (STL Robustness [29, Def. 3]) *The robustness $\rho_\varphi(\omega, k)$ of an STL formula φ (see (2)) with respect to a signal ω at time step k is defined as:*

$$\begin{aligned} \rho_{\neg\varphi}(\omega, k) &:= -\rho_\varphi(\omega, k), \\ \rho_{\varphi_1 \vee \varphi_2}(\omega, k) &:= \max(\rho_{\varphi_1}(\omega, k), \rho_{\varphi_2}(\omega, k)), \\ \rho_{\mathbf{F}_{[a, b]}\varphi}(\omega, k) &:= \max_{k' \in [k+a, k+b]} (\rho_\varphi(\omega, k')), \\ \rho_{\mathbf{G}_{[a, b]}\varphi}(\omega, k) &:= \min_{k' \in [k+a, k+b]} (\rho_\varphi(\omega, k')). \end{aligned}$$

C. Definitions for Trajectory Repair

Without loss of generality, we assume from now on that all STL formulas are expressed in negation normal form (NNF) [77, Sec. IV.A]¹, where negations are restricted to predicates and are omitted in the definitions for simplicity. To establish an upper bound for determining the branching step k_{cut} , where the associated state is the *cut-off state* [72, Def. 1], we define:

Definition 2 (Time-To-Violation [72, Def. 4]) *The time-to-violation TV_φ for a trajectory originating from \mathbf{x}_0 with the input $\mathbf{u}_{[0, h-1]}$ with respect to an STL formula φ is defined as:*

$$\begin{aligned} \text{TV}_p(\mathbf{u}_{[0, h-1]}, k) &:= \begin{cases} k & \text{if } \chi(k, \mathbf{x}_0, \mathbf{u}_{[0, k-1]}) \not\models p, \\ \infty & \text{otherwise,} \end{cases} \\ \text{TV}_{\varphi_1 \vee \varphi_2}(\mathbf{u}_{[0, h-1]}, k) &:= \max(\text{TV}_{\varphi_1}(\mathbf{u}_{[0, h-1]}, k), \\ &\quad \text{TV}_{\varphi_2}(\mathbf{u}_{[0, h-1]}, k)), \\ \text{TV}_{\mathbf{F}_{[a, b]}\varphi}(\mathbf{u}_{[0, h-1]}, k) &:= \max_{k+a \leq k' \leq k+b} \text{TV}_\varphi(\mathbf{u}_{[0, h-1]}, k'), \\ \text{TV}_{\mathbf{G}_{[a, b]}\varphi}(\mathbf{u}_{[0, h-1]}, k) &:= \min_{k+a \leq k' \leq k+b} \text{TV}_\varphi(\mathbf{u}_{[0, h-1]}, k'). \end{aligned}$$

With this, we formally define:

Definition 3 (Time-To-Comply [72, Def. 5]) *The time-to-comply TC_φ is the latest time step before TV_φ at which a trajectory complying with φ exists:*

$$\begin{aligned} \text{TC}_\varphi(\mathbf{u}_{[0, h-1]}^{\text{ini}}) &:= \max \left(\left\{ -\infty \right\} \cup \left\{ k \in [0, \text{TV}_\varphi(\mathbf{u}_{[0, h-1]}^{\text{ini}}, 0)] \right\} \right) \\ &\quad \exists \mathbf{u}_{[k, h-1]}: \forall k' \in [k, h-1]: \mathbf{u}_{k'} \in \mathcal{U}_{k'}, \\ &\quad \text{TV}_\varphi([\mathbf{u}_{[0, k-1]}^{\text{ini}}, \mathbf{u}_{[k, h-1]}], 0) = \infty \Big). \end{aligned}$$

Hereafter, we assume that TV_φ and TC_φ are evaluated at time step 0 and omit their input dependency for brevity. If no violation of φ occurs, then $\text{TC}_\varphi = \text{TV}_\varphi = \infty$. Fig. 3 illustrates example signals that violate provided formulas. Finally, we define reachable sets, which help us to find rule-compliant trajectories starting from the cut-off state:

¹Any STL formula can be converted to NNF [77, Prop. 2].

	● rule-compliant state		● rule-violating state		
k	0	1	2	3	4
φ_1	●	●	●	●	●
φ_2	●	●	●	●	●
TV_{φ_1}	∞	∞	∞	3	4
TV_{φ_2}	∞	∞	2	3	4
$\text{TV}_{\varphi_1 \vee \varphi_2}$	∞	∞	∞	3	4
$\text{TV}_{\mathcal{F}(\varphi_1 \vee \varphi_2)}$	∞	∞	∞	4	4
$\text{TV}_{\mathcal{G}(\varphi_1 \vee \varphi_2)}$	3	3	3	3	4

Fig. 3: Example computations of TV_{φ} . A circle represents a state, with its marking indicating whether the formula is satisfied or violated.

Definition 4 (Specification-Compliant Reachable Sets [36, Sec. II.C]) The exact specification-compliant reachable set \mathcal{R}_k^e at time step k is the set of states that can be reached from the set of initial states \mathcal{X}_0 while complying with the specification φ from time step 0 to k :

$$\mathcal{R}_k^e(\mathcal{X}_0, \varphi) := \left\{ \chi(k, \mathbf{x}_0, \mathbf{u}_{[0, k-1]}) \mid \exists \mathbf{x}_0 \in \mathcal{X}_0, \forall k' \in [0, k], \right. \\ \left. \exists \mathbf{u}_{k'} \in \mathcal{U}_{k'} : \chi([0, k'], \mathbf{x}_0, \mathbf{u}_{[0, k'-1]}) \models \varphi \right\}.$$

D. Problem Formulation

We focus on traffic rules formalized in STL, where the only difference from MTL is that atomic propositions σ in MTL have to be expressed as predicates p in STL [76]. Once χ^{ini} violates a rule φ , i.e., $\text{TV}_{\varphi} \neq \infty$, our repairer aims to solve²:

$$\min_{\mathbf{u}([k_{\text{cut}}, h-1])} \sum_{\tau=k_{\text{cut}}}^h J(\mathbf{x}_{\tau}, \mathbf{u}_{\tau}) \quad (3a)$$

subject to

$$k_{\text{cut}} = \arg \max \{k \in [0, \text{TV}_{\varphi}] \mid \chi([0, k], \mathbf{x}_0, \mathbf{u}_{[0, k-1]}^{\text{ini}}) \models \varphi \wedge \mathcal{R}_h^e(\mathcal{X}_k^{\text{ini}}, \varphi) \neq \emptyset\}, \quad (3b)$$

$$\forall \tau \in [0, k_{\text{cut}}]: \mathbf{x}_{\tau} = \mathbf{x}_{\tau}^{\text{ini}}, \quad (3c)$$

$$\forall \tau \in [k_{\text{cut}}, h-1]: (1), \mathbf{u}_{\tau} \in \mathcal{U}_{\tau}, \quad (3d)$$

$$\forall \tau \in [k_{\text{cut}}+1, h]: \mathbf{x}_{\tau} \in \mathcal{R}_{\tau}^e(\mathcal{X}_{k_{\text{cut}}}^{\text{ini}}, \varphi). \quad (3e)$$

Informally, our first goal is to preserve the maximum rule-compliant portion of the initial trajectory unchanged up to k_{cut} , while guaranteeing the existence of specification-compliant reachable sets from k_{cut} onward (cf. (3b) and (3c)). Subsequently, we optimize the input trajectory $\mathbf{u}([k_{\text{cut}}, h-1])$ under the system constraints in (3d), minimizing the cost function J and ensuring rule compliance by maintaining the solution within the reachable sets in (3e).

III. OVERVIEW OF THE TRAJECTORY REPAIR APPROACH

Within the outermost temporal operator, traffic rules are typically formalized to comprehensively cover all relevant situations, often expressed through disjunctions or implications [17]–[19]. Consequently, satisfying only parts of the formula is sufficient to ensure that the entire formula is satisfied. To this

²For multiple violated rules $\varphi_1, \varphi_2, \dots, \varphi_{n_v}$, they are conjoined using \wedge as $\varphi = \bigwedge_{v=1}^{n_v} \varphi_v$. The corresponding TV_{φ} is defined as the minimum value among those assigned to the rules (cf. Def. 2), i.e., $\text{TV}_{\varphi} = \min_{v \leq n_v} \text{TV}_{\varphi_v}$.

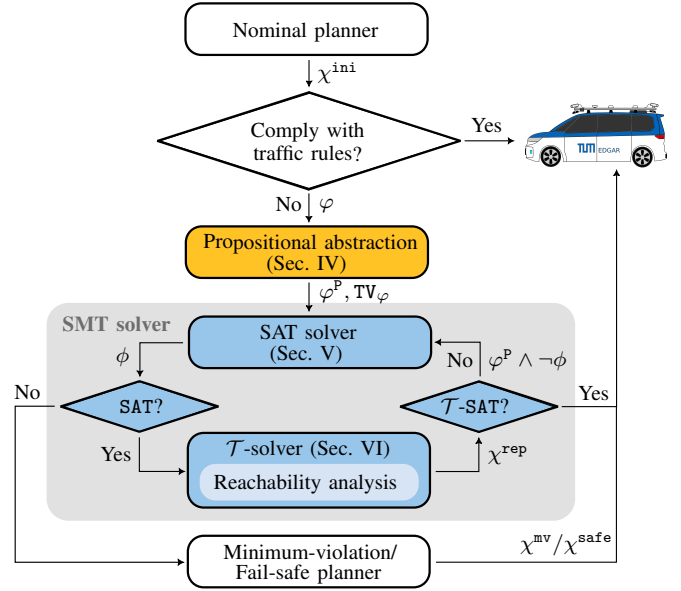


Fig. 4: Trajectory repair flowchart for a given nominal planner.

end, we use a lazy SMT solver [78], which combines a SAT solver and a \mathcal{T} -solver, to solve φ by automatically reasoning about smaller subformulas derived from its abstraction.

Fig. 4 presents an overview of our trajectory repair framework running in every planning cycle. Our repair approach is implemented as an additional layer, together with a traffic rule monitor, between the nominal planner and the control layer. Our framework is not tailored to any specific nominal planner and takes as input the trajectory χ^{ini} for the ego vehicle, the violated traffic rules φ , and the environment model. The environment model includes the road network \mathcal{L} and the rule-relevant obstacles \mathcal{B} with their predicted most likely behaviors. The output is χ^{rep} that complies with φ .

Our framework works as follows: Offline, we abstract the STL formula of formalized traffic rules to a propositional formula in conjunctive normal form (CNF) (see Sec. IV). In the online repair process, the framework leverages the abstraction φ^{P} of the violated rules φ to compute TV_{φ} (cf. Def. 2) and to initiate the SMT solver, starting with the SAT solver determining whether the abstracted problem is satisfiable, aka SAT (see Sec. V). If the SAT solver finds a satisfying assignment ϕ , the \mathcal{T} -solver computes the cut-off state and the reachability analysis to solve (3), substituting φ with ϕ (see Sec. VI). Note that the computation of the reachable sets in (3e) is expedited by satisfying only parts of φ , which may become more restrictive when approximations are introduced in the abstraction process. If successful, it generates the repaired trajectory χ^{rep} , referred to as \mathcal{T} -SAT. Otherwise, the framework refines the propositional abstraction φ^{P} by adding ϕ as a conflicting clause $\neg\phi$ and iterates the process. If the SAT solver ultimately proves the problem unsatisfiable, the framework concludes that no feasible repaired trajectory exists. In such a scenario, minimum-violation motion planning [79] complements our approach by offering a solution χ^{mv} that minimizes the extent of required rule relaxation. Another alternative is a fail-safe trajectory χ^{safe} , which can be executed to ensure safety for an infinite time horizon [69].

IV. PROPOSITIONAL TRAFFIC RULE ABSTRACTION

Our goal is to abstract the violated rules offline into a propositional logic formula that is sufficiently expressive for the SMT solver, while enabling effective online trajectory repair. To achieve this, we generalize the approach outlined in [72] by incorporating formula rewriting (see Sec. IV-A), distributive decomposition (see Sec. IV-B), and CNF conversion (see Sec. IV-C).

A. Formula Rewriting

To obtain a more compact formula with reduced nesting, each STL formula φ is rewritten into NNF φ^F [77].

Running Example: Consider the stop line rule φ_{IN1} from [19]: *The ego vehicle must stop in front of the associated stop line for at least a duration of t_{slw} before entering the intersection.* This rule is formalized in STL as follows:

$$\begin{aligned} \varphi_{\text{IN1}} = \mathbf{G} \left(\right. & \left(\text{passing_stop_line}(\mathbf{x}_{\text{ego}}) \right. \\ & \wedge \text{at_traffic_sign_stop}(\mathbf{x}_{\text{ego}}) \\ & \wedge \neg \text{relevant_traffic_light}(\mathbf{x}_{\text{ego}}) \\ & \Rightarrow \mathbf{O} \left(\mathbf{H}_{[0, t_{\text{slw}}]} \left(\text{stop_line_in_front}(\mathbf{x}_{\text{ego}}) \right. \right. \\ & \quad \left. \left. \wedge \text{in_standstill}(\mathbf{x}_{\text{ego}}) \right) \right) \left. \right), \end{aligned} \quad (4)$$

with

$$\begin{aligned} \text{passing_stop_line}(\mathbf{x}_{\text{ego}}) &:= \mathbf{P} \left(\text{stop_line_in_front}(\mathbf{x}_{\text{ego}}) \right) \\ &\wedge \neg \text{stop_line_in_front}(\mathbf{x}_{\text{ego}}). \end{aligned}$$

After rewriting, we obtain φ_{IN1}^F in NNF as:

$$\begin{aligned} \varphi_{\text{IN1}}^F = \mathbf{G} \left(\mathbf{P} \left(\neg \text{stop_line_in_front}(\mathbf{x}_{\text{ego}}) \right. \right. \\ \vee \text{stop_line_in_front}(\mathbf{x}_{\text{ego}}) \\ \vee \neg \text{at_traffic_sign_stop}(\mathbf{x}_{\text{ego}}) \\ \vee \text{relevant_traffic_light}(\mathbf{x}_{\text{ego}}) \\ \vee \mathbf{O} \left(\mathbf{H}_{[0, t_{\text{slw}}]} \left(\text{stop_line_in_front}(\mathbf{x}_{\text{ego}}) \right. \right. \\ \quad \left. \left. \wedge \text{in_standstill}(\mathbf{x}_{\text{ego}}) \right) \right) \left. \right). \end{aligned} \quad (5)$$

B. Distributive Decomposition

To further decompose φ^F into subformulas interconnected by disjunctions and conjunctions, denoted as φ^D , we utilize the distributive properties of temporal operators [80, Sec. 3.6] [81, Prop. 1]. For instance, for \mathbf{G} , we have:

$$\begin{aligned} \mathbf{G}(\varphi_1 \wedge \varphi_2) &\equiv \mathbf{G}(\varphi_1) \wedge \mathbf{G}(\varphi_2), \\ \mathbf{G}(\varphi_1 \vee \varphi_2) &\equiv \mathbf{G}(\varphi_1) \vee \mathbf{G}(\varphi_2)^3. \end{aligned} \quad (6)$$

Running Example: Applying distributive decomposition, we reformulate (5) as:

$$\varphi_{\text{IN1}}^D \equiv \mathbf{G} \left(\mathbf{P} \left(\neg \text{stop_line_in_front}(\mathbf{x}_{\text{ego}}) \right) \right)$$

³The reversed entailment symbol \equiv indicates that the formula on the right overapproximates the formula on the left.

$$\begin{aligned} &\vee \mathbf{G} \left(\text{stop_line_in_front}(\mathbf{x}_{\text{ego}}) \right) \\ &\vee \mathbf{G} \left(\neg \text{at_traffic_sign_stop}(\mathbf{x}_{\text{ego}}) \right) \\ &\vee \mathbf{G} \left(\text{relevant_traffic_light}(\mathbf{x}_{\text{ego}}) \right) \\ &\vee \mathbf{G} \left(\mathbf{O} \left(\mathbf{H}_{[0, t_{\text{slw}}]} \left(\text{stop_line_in_front}(\mathbf{x}_{\text{ego}}) \right. \right. \right. \\ &\quad \left. \left. \wedge \mathbf{H}_{[0, t_{\text{slw}}]} \left(\text{in_standstill}(\mathbf{x}_{\text{ego}}) \right) \right) \right). \end{aligned} \quad (7)$$

Remark 1 As each subformula typically corresponds to a maneuver or a traffic condition (see (7) and Sec. VI-A), the approximation in (6) neglects scenarios where the vehicle frequently changes maneuvers or traffic conditions shift rapidly – a situation that is uncommon over short planning horizons [2, Sec. II.B]. Therefore, the overapproximation has minimal impact on repair performance, as validated in [72, Sec. V.D].

C. CNF Conversion

Subformulas in φ^D connected by logical connectives are replaced by propositional variables σ_j , $j \in \mathbb{N}_+$, while those involving nested temporal operators are retained as intact units to preserve their structural integrity. This selective substitution simplifies the transformation of φ^D into an equivalent propositional formula φ^P in CNF, suitable for SAT solvers, using techniques such as the *Tseitin* transformation [82].

Running Example: After converting φ_{IN1}^D in (7) in CNF, the input for the SAT solver of rule φ_{IN1} is:

$$\varphi_{\text{IN1}}^P = \sigma_1 \vee \sigma_2 \vee \sigma_3 \vee \sigma_4 \vee \sigma_5, \quad (8)$$

with

$$\begin{aligned} \sigma_1 &:= \mathbf{G} \left(\mathbf{P} \left(\neg \text{stop_line_in_front}(\mathbf{x}_{\text{ego}}) \right) \right), \\ \sigma_2 &:= \mathbf{G} \left(\text{stop_line_in_front}(\mathbf{x}_{\text{ego}}) \right), \\ \sigma_3 &:= \mathbf{G} \left(\neg \text{at_traffic_sign_stop}(\mathbf{x}_{\text{ego}}) \right), \\ \sigma_4 &:= \mathbf{G} \left(\text{relevant_traffic_light}(\mathbf{x}_{\text{ego}}) \right), \\ \sigma_5 &:= \mathbf{G} \left(\mathbf{O} \left(\mathbf{H}_{[0, t_{\text{slw}}]} \left(\text{stop_line_in_front}(\mathbf{x}_{\text{ego}}) \right. \right. \right. \\ &\quad \left. \left. \wedge \mathbf{H}_{[0, t_{\text{slw}}]} \left(\text{in_standstill}(\mathbf{x}_{\text{ego}}) \right) \right) \right). \end{aligned}$$

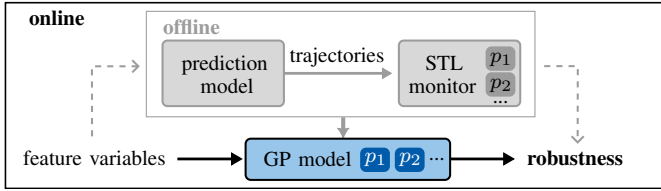
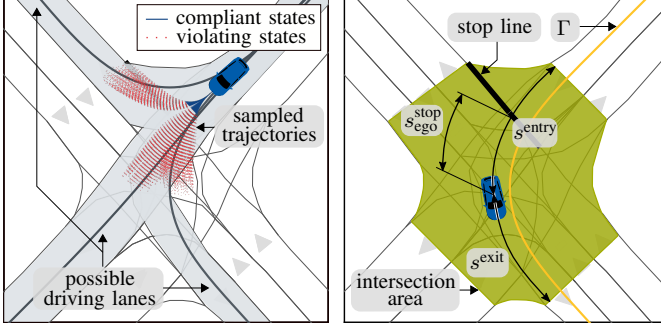
The violating truth assignments for the propositions in φ_{IN1}^P are $\llbracket \sigma_1 \rrbracket = \llbracket \sigma_2 \rrbracket = \llbracket \sigma_3 \rrbracket = \llbracket \sigma_4 \rrbracket = \llbracket \sigma_5 \rrbracket = \perp$.

V. SAT SOLVER

We employ the popular Davis–Putnam–Logemann–Loveland (DPLL) algorithm [83] to solve the Boolean satisfiability of φ^P online. Since the robustness quantifies the extent of violation or satisfaction, it can serve as a prioritization heuristic to determine the order of evaluated atomic propositions. The evaluation of STL robustness fundamentally relies on the robustness of predicates, which, however, is not included in Def. 1. Therefore, we begin by computing the model predictive robustness for the predicates in Sec. V-A, followed by the SAT solving process in Sec. V-B.

A. Model Predictive Robustness

The evaluation of robustness for STL formulas fundamentally relies on the robustness of predicates. To incorporate the dynamics of underlying system models (e.g., (1)) and streamline robustness evaluation across various predicates, we


 (a) Computation scheme for the predicates p_1 and p_2 .


(b) Prediction model.

(c) Feature variables.

Fig. 5: Computation of model predictive robustness. (a) illustrates the computation scheme for both offline and online modes. (b) displays the trajectory sampling results, where the states are labeled according to the predicate $\text{stop_line_in_front}(x_{\text{ego}})$. (c) presents selected feature variables relevant to intersections.

use model predictive robustness. The fundamental concept of model predictive robustness is to systematically assess the model capability for adhering to rule predicates. We now present the overall algorithm for computing robustness step by step, including details on adapting predicates for different types of roads.

1) *Overall Algorithm*: An accurate distribution of future vehicle behaviors is essential [84, (5)]; however, obtaining it is nontrivial. Therefore, we divide the computation of model predictive robustness into two stages: offline learning incorporating approximations and online inference (cf. Fig. 5a).

The robustness is computed offline using real traffic data. To effectively explore the configuration space, a Monte Carlo simulation is used to sample a representative set of potential future states \mathcal{X}^{MC} over a finite prediction horizon, as described in [84, Sec. III.D] (see Fig. 5b). Future trajectories of other traffic participants are represented by recorded trajectories from the dataset. For each predicate p , model predictive robustness is computed by evaluating the relative frequency of future compliant states \mathcal{X}^c with an STL monitor [84, Def. 2]⁴:

$$\rho_p(\omega, k) := \begin{cases} \frac{|\mathcal{X}^c|}{|\mathcal{X}^{\text{MC}}|} & \text{if } \alpha(\omega_k) > 0, \\ -\frac{|\mathcal{X}^{\text{MC}}| - |\mathcal{X}^c|}{|\mathcal{X}^{\text{MC}}|} & \text{otherwise,} \end{cases}$$

with the sign indicating whether p is satisfied or violated at time step k . Subsequently, pairs of feature variables that encompass relevant vehicular and environmental information based on ω_k (see Tab. I) together with their corresponding robustness values $\rho_p(\omega, k)$ are stored. These stored pairs are then used to train individual Gaussian Process (GP) regression

⁴For the sake of brevity, we omit the normalization step.

TABLE I: Feature variable definitions. All values presented are in SI units and at time step k unless otherwise specified. To compute Δ_b or $\Delta_{\mathcal{L}}$, we use the signed distance from the vehicle center to its closest point at the road boundary b or the bounds of the lanelets \mathcal{L}_{dir} .

Feature variable	Description	Location
Rule-related		
$2\llbracket p_k \rrbracket - 1$	characteristic function ⁵ [84, Def. 1]	all
Ego-vehicle-related		
$l_{\text{ego}}, w_{\text{ego}}$	vehicle length and width	all
$x_{\text{ego}}, u_{\text{ego}}$	state and input, see (1)	all
$\Delta_{\mathcal{L}_1, \text{ego}}, \Delta_{\mathcal{L}_r, \text{ego}}$	left and right distance to the left and right boundary of the lanelets \mathcal{L}_{dir}	all
$\Delta_{b_l, \text{ego}}, \Delta_{b_r, \text{ego}}$	distance to the left and right road boundary	interstates
$s_{\text{ego}}^{\text{entry}}, s_{\text{ego}}^{\text{exit}}$	longitudinal distances to the intersection area	intersections
$s_{\text{ego}}^{\text{stop}}$	longitudinal distance to the stop line	intersections
Other-vehicle-related		
$l_{\text{obs}}, w_{\text{obs}}$	vehicle length and width	all
x_{obs}	state, see (1)	all
$\Delta_{\mathcal{L}_1, \text{obs}}, \Delta_{\mathcal{L}_r, \text{obs}}$	left and right distance to the left and right boundary of the lanelets \mathcal{L}_{dir}	all
$\Delta_{b_l, \text{obs}}, \Delta_{b_r, \text{obs}}$	distance to the left and right road boundary	interstates
$s_{\text{obs}}^{\text{entry}}, s_{\text{obs}}^{\text{exit}}$	longitudinal distances to the intersection area	intersections
Ego-other-relative		
$\Delta s_{\text{ego}}, \Delta d_{\text{ego}}$	relative longitudinal and lateral distance along Γ_{ego}	all
$\Delta s_{\text{obs}}, \Delta d_{\text{obs}}$	relative longitudinal and lateral distance along Γ_{obs}	intersections
$\Delta v_s, \Delta v_d$	relative velocity in the longitudinal and lateral directions along respective Γ of each vehicle	all

models for each predicate p , improving computational efficiency and reducing noise in robustness computation. These pretrained models are later utilized in online applications with the same feature variables.

2) *Extension to Intersections*: As the work [84] primarily focuses on interstates, its application to intersections necessitates careful adjustments to both the trajectory sampling process in the prediction model and the feature variables.

a) *Trajectory Sampling*: It is important to note that vehicles at intersections exhibit a greater variety of velocity changes compared to those on interstates. Therefore, when the velocity falls below a certain threshold $v_{\text{switch}} \in \mathbb{R}_+$, the lateral trajectory generation is integrated with the longitudinal motion rather than being treated as an independent process [11, Rem. 5]. Furthermore, the selection of the reference path has to account for all possible driving directions within the road networks, as shown in Fig. 5b.

b) *Feature Variables*: Given the increased complexity of the road network at intersections compared to interstates,

⁵The function equals 1 when $\llbracket p_k \rrbracket$ is \top ; otherwise, it equals -1 .

TABLE II: Description of time-to-maneuvers and the corresponding predicate categories.

Time-to-maneuver [85]	Description	Category [34]	Predicates [17], [19]
Time-to-brake (TTB)	Full braking with maximum deceleration.	Longitudinal position, velocity	in_conflict_area, keeps_lane_speed_limit, stop_lane_in_front, ...
Time-to-kick-down (TTK)	Full acceleration until reaching the maximum velocity and then maintaining the velocity.		
Time-to-steer (TTS)	Full steering to reach a certain lateral offset or a specified orientation change.	Lateral position	in_same_lane, left_of, turning_left, ...
Time-to-maintain-velocity (TTMV)	Maintaining a constant velocity.	Acceleration	brakes_abruptly, ...

especially regarding regulatory elements and intersection labels, it is necessary to extend the features in [84, Tab. I]. Tab. I summarizes the updated feature variables, categorized according to various locations, with some details provided as follows: To effectively analyze intersection-related features, the intersection area is characterized as the region consisting of lanelets that are mutually accessible to vehicles approaching the intersection from various directions [86] and shown in Fig. 5c. Consequently, the distance to the intersection area of a vehicle is represented by the longitudinal distance to its entry and exit points, denoted as s^{entry} and s^{exit} , respectively, along its reference path Γ . Furthermore, if stop lines are present within \mathcal{L}_{dir} , the longitudinal distance $s_{\text{ego}}^{\text{stop}}$ from the ego vehicle to the nearest one along Γ is chosen. Otherwise, $s_{\text{ego}}^{\text{stop}}$ is assigned a default value [86, Sec. III.A]. Given that the other vehicle might travel in different directions at intersections, we additionally measure the relative distance between the vehicles along the reference path of the other vehicle Γ_{obs} , denoted by Δs_{obs} and Δd_{obs} .

B. SAT Solving

In the DPLL algorithm, a partial solution ϕ – consisting of truth assignments for a subset of propositions required to satisfy φ^{P} – is incrementally constructed. To prioritize propositions whose values are easy to change, they are sorted in ascending order based on their absolute robustness values $|\rho_{\sigma_j}|$ over the time interval $[\text{TV}_{\varphi}, h]$, where the rule violation occurs (cf. Def. 2). The DPLL algorithm systematically explores the sorted propositions by iteratively assigning truth values, propagating constraints, and backtracking when conflicts arise [87].

Running Example: We assume that the ranked order of the propositions in (8) is $\sigma_2 < \sigma_1 < \sigma_5 < \sigma_3 < \sigma_4$. In the first iteration of the SMT solver, the DPLL algorithm produces the partial solution $\llbracket \sigma_2 \rrbracket = \top$, meaning the requirement is $\mathbf{G}(\text{stop_line_in_front}(x_{\text{ego}}))$.

VI. T-SOLVER

In the \mathcal{T} -Solver, we solve (3) by replacing φ with the SAT solution ϕ and determining the cut-off state of the initial trajectory at TC_{ϕ} . Following [72, Alg. 2], we first compute TC_{ϕ} based on ϕ and TV_{φ} . Next, we compute the specification-compliant reachable sets starting from TC_{ϕ} in Sec. VI-B, followed by solving a convex optimization problem to obtain the repaired trajectory in Sec. VI-C.

A. Time-To-Comply Computation

Since considering all possible reachable states to calculate the exact TC_{ϕ} (cf. Def. 3) is computationally intractable, we

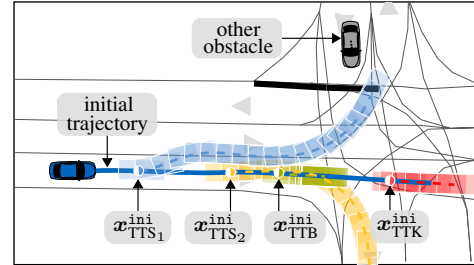


Fig. 6: Illustration of evasive maneuvers in Tab. II, depicting the starting points of each maneuver along with their associated occupancies. The TTS is demonstrated by reaching a specified lateral offset (TTS₁) and achieving a defined orientation change (TTS₂).

employ an underapproximation that focuses on a selected set of maneuvers \mathcal{M} [72, Sec. IV.C]. The goal is to alter the truth assignment of the atomic propositions $\phi_r \subseteq \phi$, which differ in their values at TV_{φ} ⁶ from the case where the propositional formula is satisfied, i.e., $\llbracket \varphi^{\text{P}} \rrbracket = \top$. The maneuvers are automatically determined by the categories relative to the domains of the predicates within ϕ_r , as outlined in Tab. II and illustrated in Fig. 6. Note that predicates within past-time temporal operators cannot guide actions for future compliance. Each maneuver is associated with a time-to-maneuver [85], representing the latest possible time at which the maneuver can still be executed to comply with φ and calculated using [88, Alg. 2]. According to Def. 3, TC_{ϕ} is then underapproximated by the maximum time-to-maneuver among the set \mathcal{M} .

Running Example: For the obtained SAT solution ϕ where $\llbracket \sigma_2 \rrbracket = \top$, the time-to-maneuvers are TTB and TTK, as the predicate $\text{stop_line_in_front}(x_{\text{ego}})$ belongs to the category of longitudinal position.

B. Specification-Compliant Reachability Analysis

After the cut-off state $x_{\text{TC}_{\phi}}^{\text{ini}}$, we adopt the approach proposed in [35], [36] to compute the reachable sets against ϕ in (3e) as the search space over the time interval $[\text{TC}_{\phi}, h]$. Since computing the exact reachable sets under specifications is infeasible for efficiency reasons [36, Sec. II.D], we use a tight overapproximation $\mathcal{R}_{k'}$ of $\mathcal{R}_{k'}^{\text{e}}$ that encloses all kinematically feasible and specification-compliant trajectories. Note that the distributivity of \mathbf{G} over \vee in (6) imposes stricter rule requirements (cf. Rem. 1). To mitigate its impact of overly shrinking the valid solution space, we follow the syntactic timing separation theorem [81, Thm. 1] and relax $\mathbf{G}_{[\text{TC}_{\phi}, h]} \varphi$

⁶We observe at TV_{φ} instead of $[\text{TV}_{\varphi}, h]$ as the violation assignments may change or resolve throughout the interval. If multiple rules $\varphi = \bigwedge_{v=1}^{n_{\varphi}} \varphi_v$ are violated, the assignments are compared individually to those at TV_{φ_v} .

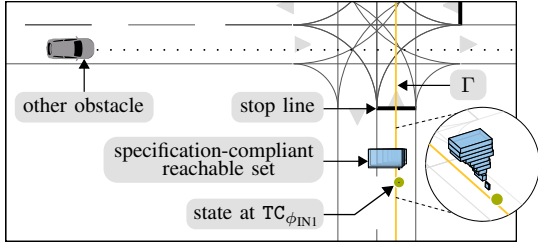


Fig. 7: Examples of specification-compliant reachable sets, which are projected onto the position domain.

in the proposition when the overapproximation is used during the propositional abstraction in Sec. IV:

$$\mathbf{G}_{[TC_\phi, h]} \varphi \equiv \mathbf{G}_{[TC_\phi, TV_\varphi]} \varphi \wedge \mathbf{G}_{[TV_\varphi, h]} \varphi \models \mathbf{G}_{[TV_\varphi, h]} \varphi,$$

with which the reachable sets remaining overapproximative. In addition, collision avoidance is included as a default specification over the entire time horizon for safety concerns by conjuncting it with the SAT solution ϕ [36]⁷. With this, we perform automaton-based model checking on the fly [36] to compute the specification-compliant reachable sets.

Running Example: Given the SAT solution $[\sigma_2] = \top$, Fig. 7 shows the computed reachable sets over the time interval $[TC_\phi, h]$ against $\mathbf{G}_{[TV_\varphi, h]}$ (`stop_line_in_front(x_{ego})`), which significantly narrow down the search space for finding repaired trajectories compared to the entire configuration space.

C. Optimization-Based Trajectory Repair

Based on the reachable sets, we first extract a driving corridor [35, Sec. II.E] with no holes by applying utility functions such as spatial coverage. Then, we formulate a convex optimization problem [89] for finding repaired trajectories with a fast convergence. Setting k_{cut} to TC_ϕ , the problem in (3) over the time interval $[TC_\phi, h]$ aligns with the problem statement and can be addressed using the approach detailed in [90], with one addition: to enhance rule compliance, we include a robustness term in J to minimize deviations from, e.g., the edges of reachable sets, where vehicle states with high robustness values are typically located. Since the reachable sets are tightly overapproximative, the computed trajectory may exhibit slight violations of φ . Thus, we only return the repaired trajectory if it is verified to be rule-compliant.

VII. EXPERIMENTAL RESULTS

We showcase the usefulness of our framework to effectively address multiple rule violations and adeptly handle complex, real-world scenarios. Following the implementation details in Sec. VII-A, we focus on repairing multiple rule violations in Sec. VII-B. We then show the scalability of our approach to intersection traffic rules in Sec. VII-C, compare it with related work in Sec. VII-D, and analyze the computation time in Sec. VII-E. Finally, we validate our method for the first time through closed-loop planning tests conducted within the realistic CARLA simulator in Sec. VII-F and in the real world in Sec. VII-G.

⁷For the interval $[0, TC_\phi]$, it is assumed that χ^{ini} has sufficient quality for execution and is collision-free.

TABLE III: General parameters for the numerical experiments (all variables are expressed in SI units).

Description	Notation and value
Model predictive robustness	
number of samples	1500
prediction horizon	1.56s
velocity sampling interval	$[\max(0, v_k - 17.25), v_k + 17.25]$
lateral position sampling interval	
high speed mode	$[d_k - 5, d_k + 5]$
low speed mode	$[d_k - 1.5, d_k + 1.5]$
derivative of lateral position	
high speed mode	$[-3, 3]$ m/s
low speed mode	$[-0.2, 0.2]$ m/s
switching velocity	$v_{switch} = 4$ m/s
Traffic rule monitoring	
waiting time duration	$t_{slw} = 3$ s (cf. (4))
time to restore a safe distance	$t_c = 3$ s (cf. (9))
waiting time, entry delay	$t_{ia} = 0.5$ s, $t_{ib} = 1$ s (cf. Sec. VII-C2)
Dataset evaluation	
time step size	$\Delta t = 0.2$ s
maximum planning horizon	$h = 20$
longitudinal and lateral weights	$[0.1, 0.1, 0.5, 1]$, robustness: -1
CARLA simulation	
time step size, planning horizon	$\Delta t = 0.1$ s, $h = 30$
replanning cycle	1.0s
Real-world experiments	
time step size, planning horizon	$\Delta t = 0.1$ s, $h = 50$
replanning cycle	0.2s

A. Implementation Details

1) *General Settings:* Our approach is implemented in Python, and simulations were conducted on a single thread using a machine equipped with an AMD EPYC 7763 64-core processor and 2TB of RAM. In our implementation, we use GPyTorch [91] to model and solve GP regression and RTAMT [92] to monitor rules and evaluate robustness. The CommonRoad-CriMe toolbox [85] is employed to derive the cut-off state, while the CommonRoad-Reach toolbox [93] is used to compute the reachable sets from that state. Finally, the Gurobi solver [94] is applied to solve the trajectory optimization problem and obtain the repaired trajectory. Tab. III lists the selected parameters, while all other parameters remain consistent with those defined in the original paper.

2) *Vehicle Models:* For model predictive robustness computation and trajectory optimization, we use the vehicle models presented in [69]. The longitudinal dynamics are represented as a fourth-order integrator, while the lateral dynamics are modeled by a linearized kinematic single-track model, with both formulated in the curvilinear coordinate system.

3) *Traffic Rules and Scenarios:* We adopt the formalized German interstate [17] and intersection [19] traffic rules. To train the GP regression model for online computation of model predictive robustness, we use scenarios derived from the highD [95] and inD [96] datasets. These drone-captured datasets

TABLE IV: Key parameters obtained during trajectory repair.

Parameter	Values
Multi-rule violation	
TV_{φ}	13 ($TV_{\varphi_{G1}} = 13$, $TV_{\varphi_{G3}} = 15$)
ρ_{σ_j} over $[TV_{\varphi}, h]$	$\sigma_1: -0.351$, $\sigma_2: -0.971$, $\sigma_3: -0.236$, $\sigma_4: -0.295$, $\sigma_5: 0.692$, $\sigma_6: 0.786$, $\sigma_7: 0.903$, $\sigma_8: -0.032$
1. iteration	ϕ $\llbracket \sigma_3 \rrbracket = \top$, $\llbracket \sigma_5 \rrbracket = \top$, $\llbracket \sigma_6 \rrbracket = \top$, $\llbracket \sigma_7 \rrbracket = \top$, $\llbracket \sigma_8 \rrbracket = \top$
✓	TC_{ϕ} $\max\{\text{TTB}, \text{TTK}, \text{TTS}\} = \text{TTB} = 12$
Stop line rule	
TV_{φ}	15
ρ_{σ_j} over $[TV_{\varphi}, h]$	$\sigma_1: -0.001$, $\sigma_2: -0.968$, $\sigma_3: -1.000$, $\sigma_4: -1.000$, $\sigma_5: -0.970$
1. iteration	ϕ , TC_{ϕ} $\llbracket \sigma_1 \rrbracket = \top$, $-\infty$
✗	
2. iteration	ϕ $\llbracket \sigma_1 \rrbracket = \perp$, $\llbracket \sigma_2 \rrbracket = \top$
✓	TC_{ϕ} $\max\{\text{TTB}, \text{TTK}\} = \text{TTB} = 12$
Priority rule	
TV_{φ}	9
ρ_{σ_j} over $[TV_{\varphi}, h]$	$\sigma_1: -0.221$, $\sigma_2: -0.628$, $\sigma_3: -0.389$, $\sigma_{10}: -0.773$, $\sigma_{11}: 0.965$, $\sigma_{12}: -0.741$, $\sigma_{13}: -0.741$, $\sigma_{14}: -0.773$, $\sigma_{15}: -1.000$
1. iteration	ϕ $\llbracket \sigma_1 \rrbracket = \top$, $\llbracket \sigma_2 \rrbracket = \top$, $\llbracket \sigma_3 \rrbracket = \top$, $\llbracket \sigma_{10} \rrbracket = \top$, $\llbracket \sigma_{14} \rrbracket = \top$
✓	TC_{ϕ} $\max\{\text{TTB}, \text{TTK}\} = \text{TTB} = 5$

provide recorded traffic data from highway and urban locations in Germany, ensuring consistency with the formalized traffic rules. During the evaluation, we convert the raw data into CommonRoad scenarios [97] using an open-source data converter⁸, with each scenario limited to a maximum duration of 4s. We focus on scenarios containing rule violations and designate the violating vehicle as the ego vehicle.

B. Multiple Traffic Rule Violations

We begin by considering a highway scenario from the highD dataset, where the initial trajectory of the ego vehicle violates multiple traffic rules. As illustrated in Fig. 8, these violations include the safe distance rule φ_{G1} and the speed limit rule φ_{G3} [17]. We combine the violated rules using a conjunction as $\varphi_{G1, G3}$:

$$\varphi_{G1, G3} = \varphi_{G1} \wedge \varphi_{G3} \quad (9)$$

with

$$\begin{aligned} \varphi_{G1} &= \mathbf{G}(\text{in_same_lane}(\mathbf{x}_{\text{ego}}, \mathbf{x}_{\text{obs}}) \wedge \text{behind}(\mathbf{x}_{\text{ego}}, \mathbf{x}_{\text{obs}}) \wedge \\ &\quad \neg \mathbf{O}_{[0, t_c]}(\text{cut_in}(\mathbf{x}_{\text{obs}}, \mathbf{x}_{\text{ego}}) \wedge \\ &\quad \quad \mathbf{P}(\neg \text{cut_in}(\mathbf{x}_{\text{obs}}, \mathbf{x}_{\text{ego}}))) \\ &\Rightarrow \text{keeps_safe_distance_prec}(\mathbf{x}_{\text{ego}}, \mathbf{x}_{\text{obs}})) \text{ and} \\ \varphi_{G3} &= \mathbf{G}(\text{keeps_lane_speed_limit}(\mathbf{x}_{\text{ego}}) \wedge \\ &\quad \text{keeps_type_speed_limit}(\mathbf{x}_{\text{ego}}) \wedge \\ &\quad \text{keeps_fov_speed_limit}(\mathbf{x}_{\text{ego}}) \wedge \end{aligned}$$

⁸<https://commonroad.in.tum.de/tools/dataset-converters>

$\text{keeps_braking_speed_limit}(\mathbf{x}_{\text{ego}})$.

By abstracting the rule formula (cf. Sec. IV), we obtain the input for the SAT solver as:

$$\varphi_{G1, G3}^P = \underbrace{(\sigma_1 \vee \sigma_2 \vee \sigma_3 \vee \sigma_4)}_{\varphi_{G1}} \wedge \underbrace{\sigma_5 \wedge \sigma_6 \wedge \sigma_7 \wedge \sigma_8}_{\varphi_{G3}},$$

$$\begin{aligned} \text{with } \sigma_1 &:= \mathbf{G}(\text{keeps_safe_distance_prec}(\mathbf{x}_{\text{ego}})), \\ \sigma_2 &:= \mathbf{G}(\neg \text{behind}(\mathbf{x}_{\text{ego}}, \mathbf{x}_{\text{obs}})), \\ \sigma_3 &:= \mathbf{G}(\neg \text{in_same_lane}(\mathbf{x}_{\text{ego}}, \mathbf{x}_{\text{obs}})), \\ \sigma_4 &:= \mathbf{G}(\mathbf{O}_{[0, t_c]}(\text{cut_in}(\mathbf{x}_{\text{obs}}, \mathbf{x}_{\text{ego}}) \\ &\quad \wedge \mathbf{P}(\neg \text{cut_in}(\mathbf{x}_{\text{obs}}, \mathbf{x}_{\text{ego}}))), \\ \sigma_5 &:= \mathbf{G}(\text{keeps_lane_speed_limit}(\mathbf{x}_{\text{ego}})), \\ \sigma_6 &:= \mathbf{G}(\text{keeps_type_speed_limit}(\mathbf{x}_{\text{ego}})), \\ \sigma_7 &:= \mathbf{G}(\text{keeps_fov_speed_limit}(\mathbf{x}_{\text{ego}})), \\ \sigma_8 &:= \mathbf{G}(\text{keeps_braking_speed_limit}(\mathbf{x}_{\text{ego}})). \end{aligned}$$

Using the SMT framework, we obtain the repaired trajectory, as shown in Fig. 8a, with its key parameters listed in Tab. IV. In the first iteration, the SAT solver suggests a change in the truth assignments of the propositions σ_3 and σ_8 , which correspond to the maneuvers of braking, accelerating, and steering. In the \mathcal{T} -solver, we determine that $TC_{\phi} = \text{TTB}$ and obtain the specification-compliant reachable sets depicted in Fig. 8b. Consequently, the ego vehicle performs a braking maneuver to comply with the violated rules, which is evident from the velocity profile in Fig. 8e.

C. Intersection Traffic Rule Violation

In this section, we demonstrate our trajectory repair approach against typical intersection rules using inD scenarios.

1) *Stop Line Rule*: Consider the stop line rule in (4), where a violation occurs if the ego vehicle fails to stop for t_{slw} behind the stop line before crossing it, as shown in Fig. 9a. In the first iteration of the repair process, the SAT solver returns the solution $\llbracket \sigma_1 \rrbracket = \top$ (cf. (8) and Tab. IV), which does not correspond to any maneuvers due to the presence of a past-time temporal operator in σ_1 . Consequently, the second iteration yields the solution $\llbracket \sigma_1 \rrbracket = \perp$, $\llbracket \sigma_2 \rrbracket = \top$, leading to braking and kick-down maneuvers, resulting in $TC_{\phi} = 12$. After performing reachability analysis and optimization-based trajectory repair, the initial trajectory is adjusted to slow down from TC_{ϕ} and come to a full stop before the stop line (cf. Fig. 9b).

2) *Priority Rule*: Next, we consider a more complex rule – rural priority rule φ_{IN4} [19], which prohibits the ego vehicle from entering an intersection if this action would pose a danger to another vehicle with the right of way:

$$\begin{aligned} \varphi_{\text{IN4}} &= \mathbf{G}(\text{obs_straight_ego_straight_obs_prio}(\mathbf{x}_{\text{obs}}, \mathbf{x}_{\text{ego}})^9 \\ &\quad \vee \text{obs_straight_ego_left_turns_obs_prio}(\mathbf{x}_{\text{obs}}, \mathbf{x}_{\text{ego}})) \end{aligned}$$

⁹ $\text{obs_straight_ego_straight_obs_prio}(\mathbf{x}_{\text{obs}}, \mathbf{x}_{\text{ego}})$ is an abbreviation of the subformula $\text{going_straight}(\mathbf{x}_{\text{obs}}) \wedge \text{going_straight}(\mathbf{x}_{\text{ego}}) \wedge \text{has_priority}(\mathbf{x}_{\text{obs}}, \mathbf{x}_{\text{ego}})$ from [19, Tab. VI], which allows us to make the formula more compact. This abbreviation format similarly applies to all combinations of turning directions.

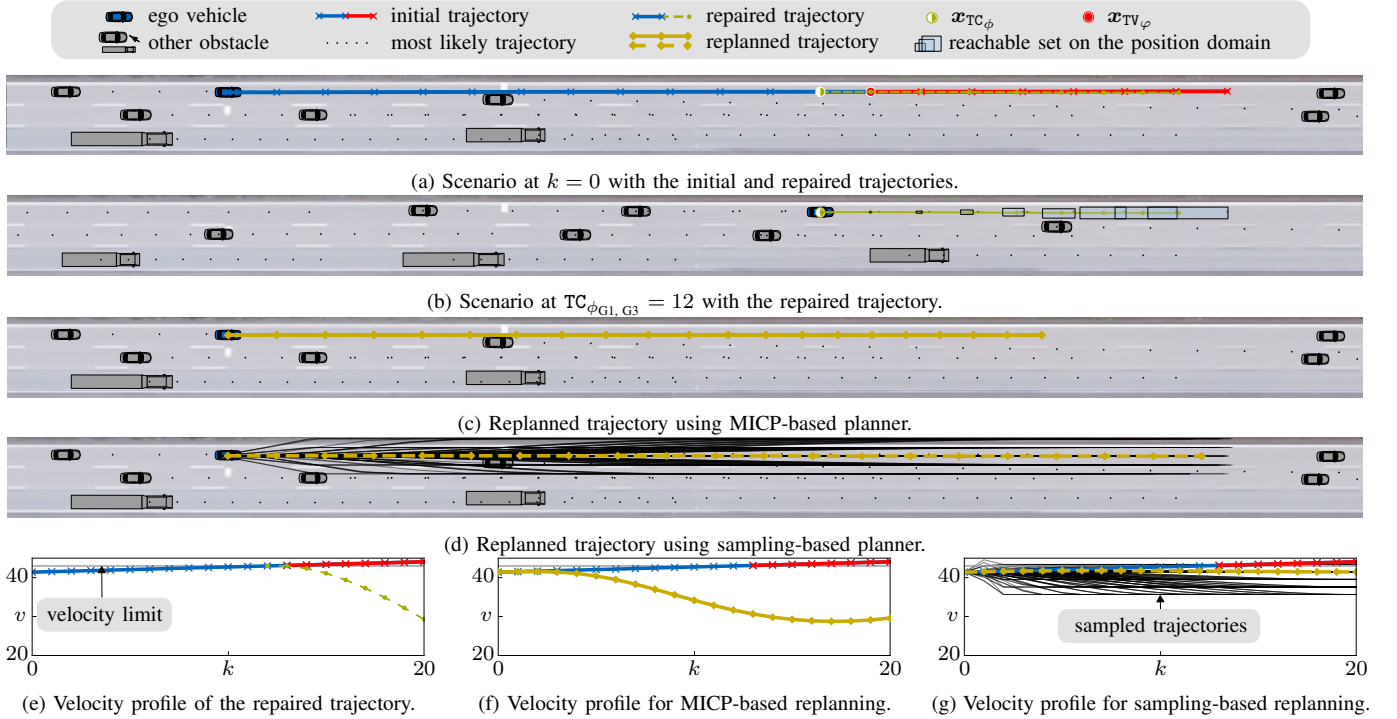


Fig. 8: Highway scenario where the ego vehicle violates safety distance and speed limit rules. (a) and (b) show the initial and repaired trajectories, with a velocity comparison in (e). (c) and (d) present the replanned trajectories using MICP-based and sampling-based planners, respectively, with their velocity profiles shown in (f) and (g).

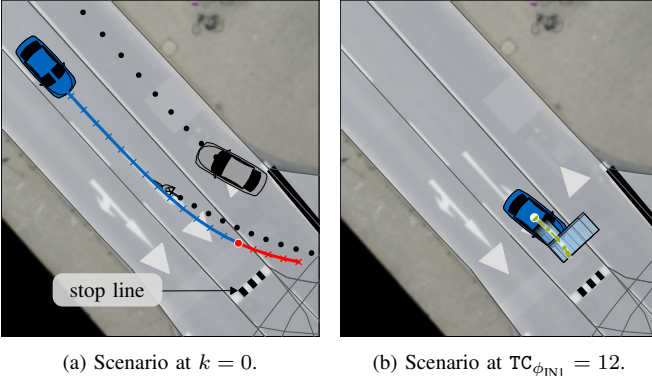


Fig. 9: Rural scenario where the initial trajectory of the ego vehicle in (a) violates the stop line rule, which is repaired by our approach in (b). The legends are the same as in Fig. 8.

$$\begin{aligned} & \vee \text{obs_straight_ego_right_turns_obs_prio}(\mathbf{x}_{\text{obs}}, \mathbf{x}_{\text{ego}}) \\ & \vee \dots \text{combinations of turning directions} \dots \\ \Rightarrow & (\mathbf{G}(\text{not_endanger_intersection}(\mathbf{x}_{\text{ego}}, \mathbf{x}_{\text{obs}})) \\ & \vee \text{-on_lanelet_with_type_intersection}(\mathbf{x}_{\text{ego}})), \end{aligned}$$

$$\begin{aligned} \text{with not_endanger_intersection}(\mathbf{x}_{\text{ego}}, \mathbf{x}_{\text{obs}}) := & \\ & (\text{in_intersection_conflict_area}(\mathbf{x}_{\text{ego}}, \mathbf{x}_{\text{obs}}) \\ \Rightarrow & (\text{-causes_braking_intersection}(\mathbf{x}_{\text{ego}}, \mathbf{x}_{\text{obs}}) \\ & \wedge \neg \mathbf{F}_{[0, t_{\text{ib}}]}(\text{in_intersection_conflict_area}(\mathbf{x}_{\text{obs}}, \mathbf{x}_{\text{ego}}))) \\ \wedge & (\text{in_intersection_conflict_area}(\mathbf{x}_{\text{obs}}, \mathbf{x}_{\text{ego}}) \\ \Rightarrow & \neg \mathbf{F}_{[0, t_{\text{ia}}]}(\text{in_intersection_conflict_area}(\mathbf{x}_{\text{ego}}, \mathbf{x}_{\text{obs}}))). \end{aligned}$$

As illustrated in Fig. 10a, the ego vehicle violates φ_{IN4} as its initial trajectory enters the conflict area – the overlapping

region of the lanes – with the rule-relevant obstacle. Following formula rewriting and distributive decomposition (cf. Sec. IV), we obtain $\varphi_{\text{IN4}}^{\text{D}}$ as:

$$\begin{aligned} \varphi_{\text{IN4}}^{\text{D}} = & (\sigma_1 \wedge \sigma_2 \wedge \sigma_3 \wedge \dots) \vee (\sigma_{10} \wedge \sigma_{13}) \vee (\sigma_{10} \wedge \sigma_{14}) \\ & \vee (\sigma_{11} \wedge \sigma_{12} \wedge \sigma_{13}) \vee (\sigma_{11} \wedge \sigma_{12} \wedge \sigma_{14}) \vee \sigma_{15}, \end{aligned}$$

with

$$\begin{aligned} \sigma_1 := & \mathbf{G}(\text{-obs_straight_ego_straight_obs_prio}(\cdot)), \\ \sigma_2 := & \mathbf{G}(\text{-obs_straight_ego_left_turns_obs_prio}(\cdot)), \\ \sigma_3 := & \mathbf{G}(\text{-obs_straight_ego_right_turns_obs_prio}(\cdot)), \\ & \dots \end{aligned}$$

$$\begin{aligned} \sigma_{10} := & \mathbf{G}(\text{-in_intersection_conflict_area}(\mathbf{x}_{\text{ego}}, \mathbf{x}_{\text{obs}})), \\ \sigma_{11} := & \mathbf{G}(\text{-causes_braking_intersection}(\cdot)), \\ \sigma_{12} := & \mathbf{G}(\neg \mathbf{F}_{[0, t_{\text{ib}}]}(\text{in_intersection_conflict_area}(\mathbf{x}_{\text{obs}}, \mathbf{x}_{\text{ego}}))), \\ \sigma_{13} := & \mathbf{G}(\text{-in_intersection_conflict_area}(\mathbf{x}_{\text{obs}}, \mathbf{x}_{\text{ego}})), \\ \sigma_{14} := & \mathbf{G}(\neg \mathbf{F}_{[0, t_{\text{ia}}]}(\text{in_intersection_conflict_area}(\mathbf{x}_{\text{ego}}, \mathbf{x}_{\text{obs}}))), \\ \sigma_{15} := & \mathbf{G}(\text{-on_lanelet_with_type_intersection}(\cdot)). \end{aligned}$$

Next, $\varphi_{\text{IN4}}^{\text{D}}$ is transformed into $\varphi_{\text{IN4}}^{\text{P}}$ in CNF, which serves as the input to the online SAT solver. After detecting the violation, the SAT solver first generates a partial solution ϕ (see Tab. IV), which serves as input for the \mathcal{T} -solver. This solution corresponds to adjustments in the truth assignments of the propositions σ_{10} and σ_{14} . After a single iteration, our approach successfully enables the ego vehicle to stop and yield to the obstacle with higher priority crossing the same intersection (see Fig. 10a and Fig. 10d).

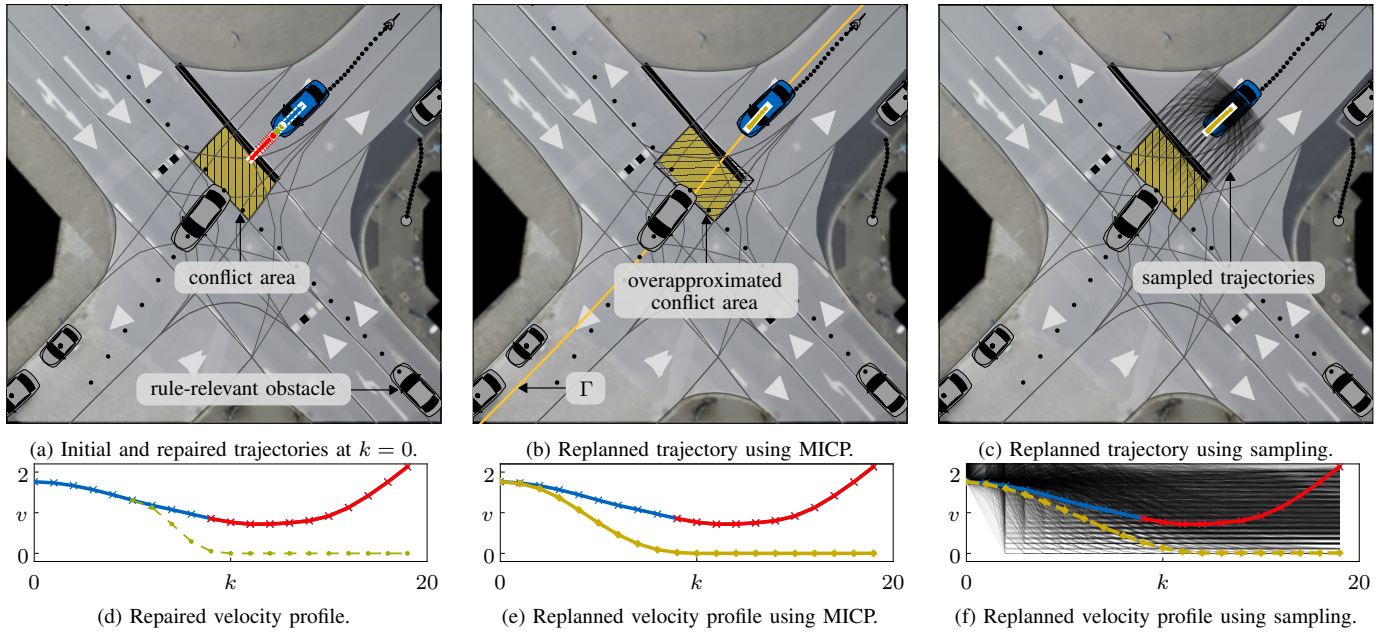


Fig. 10: Intersection scenario where the initially planned trajectory for the ego vehicle violates the priority rule by entering the conflict area without yielding to a higher-priority obstacle. (a) and (d) depict the initial and repaired configurations, respectively, while (b) and (e), as well as (c) and (f), illustrate the replanned trajectories. The same legends from Fig. 8 are used for consistency.

TABLE V: Computation time comparison between trajectory repair and replanning, with the best performance highlighted in bold.

	Multi-violation ↓	Stop line ↓	Priority ↓
repair	127 ms	88 ms	193 ms
replan using MICP	1708 ms	699 ms	2401 ms
replan using sampling	1408 ms	218 ms	1812 ms

D. Comparison with Related Work

To further support our claims in Sec. I, we compare our approach with a full trajectory replanning strategy, highlighting the advantages of partially adapting the initial trajectory.

1) *Replanning Using Mixed-Integer Convex Programming:* The first comparison is with a state-of-the-art temporal logic motion planner¹⁰ based on mixed-integer convex programming (MICP) [98], [99], which encodes STL specifications in NNF over convex predicates using binary variables. To align with the repair setup (cf. Sec. VII-A2), the dynamics of the ego vehicle are modeled as fourth-order integrators for both longitudinal and lateral directions along Γ . For simple predicates that map state variables to real values, we parameterize them based on the definition provided in [100, Sec. IV.C], facilitating the formulation of convex constraints. In more complex cases, we employ approximations to evaluate robustness while maintaining the soundness of the approach [84, Prop. 1]. For instance, for $\neg \text{in_intersection_conflict_area}(\cdot)$, we overapproximate the exact conflict area with a polygon defined by its extreme (maximum and minimum) vertex coordinates in the curvilinear coordinate system (cf. Fig. 10b). The robustness is then computed as the signed distance to its longitudinal and lateral bounds. Furthermore, to primarily investigate the impact of the rules on computation time, we limit the collision

avoidance constraints to obstacles within the same lane \mathcal{L}_{dir} as the ego vehicle. For solving the optimization problem, we employ Gurobi [94], consistent with our setup.

Fig. 8c and Fig. 10b show the replanned results using MICP for the rules $\varphi_{G1, G3}$ and φ_{IN4} , respectively. From Tab. V, it is evident that the runtime increases with the complexity of the formula. This is particularly noticeable for rule $\varphi_{G1, G3}$, where the nonlinear predicate `keeps_safe_distance_prec(\cdot)` is approximated using piecewise-linear functions [100, Sec. IV.C], resulting in a higher number of constraints. In comparison, our trajectory repair approach consistently produces feasible solutions in significantly less time, regardless of the formula length. Moreover, the MICP optimization problem, which simultaneously maximizes the robustness of rule compliance and minimizes the cost function, generates velocity profiles comparable to those obtained through trajectory repair. This demonstrates consistency in outcomes across both approaches (cf. Fig. 8 and Fig. 10).

We further evaluate our approach by comparing it to the MICP-based replanning method across 150 randomly selected highD and inD scenarios (cf. Sec. VII-A3), with the runtime performance depicted in Fig. 11. Our approach demonstrates exceptional efficiency, achieving a runtime that is 90.7% faster than MICP-based replanning. This remarkable performance is driven by the decomposition of rules into smaller subformulas and the effective application of convex optimization techniques. Although the runtime varies with the scenario configuration, particularly with the length of the violation segments, i.e., $h - TV_\varphi$, the worst-case runtime for our method remains superior to that of the MICP approach. Moreover, 33.3% of the MICP replanning attempts for the φ_{IN4} violation fail due to the excessive overapproximation of the conflict area, resulting in an empty solution space – an issue that does not occur with our approach.

¹⁰The implementation is based on <https://github.com/vincekurtz/stlpy>.

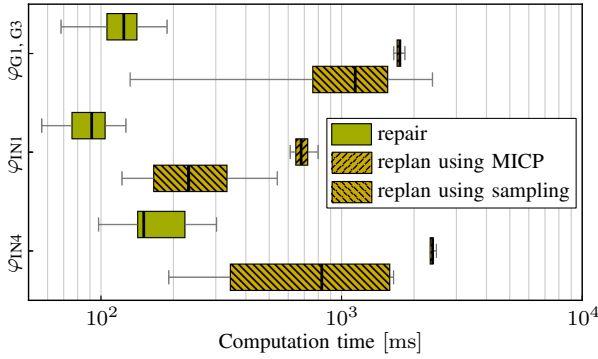


Fig. 11: Comparison of runtime performance between our approach and MICP-based and sampling-based replanning. Outliers are omitted from the box plot for enhanced clarity.

2) *Replanning Using Sampling-Based Planner*: We adapt the popular sampling-based motion planner¹¹ described in [11], which generates a finite set of quintic polynomials as candidate trajectories connecting the current state to sampled goal states. The polynomials are then ranked based on a cost function, with each being checked for feasibility – including drivability and collision avoidance – and compliance with the violated rules. The planner terminates upon identifying a feasible solution, which is the trajectory with the minimum cost function that satisfies these checks, and returns it as the replanned trajectory.

The exemplary replanned results for rules $\varphi_{G1, G3}$ and φ_{IN4} are shown in Fig. 8d and Fig. 10c, respectively, each require over 1s (cf. Tab. V). For $\varphi_{G1, G3}$, although a sampled trajectory that maintains the initial velocity is valid (cf. Fig. 8g), it is not prioritized during the checking process because the high initial acceleration of the ego vehicle is penalized by the cost function. In the case of φ_{IN4} , the initial use of 270 samples fails to yield a feasible trajectory, as the ego vehicle is already nearing the conflict area, resulting in a limited solution space. Moreover, the scenario requires the vehicle to decelerate to a full stop; however, the polynomial velocity profile imposes further limitations on the available options (cf. Fig. 10f). Therefore, the sample number is gradually increased to 5508 before a solution is found. In contrast, our approach finds feasible trajectories with a stable runtime across all three examples, each taking less than 200ms.

Next, we compare our approach with the sampling-based replanning method across the selected 150 scenarios. As shown in Fig. 11, the runtime deviation for the sampling-based approach is significantly greater than that of trajectory repair, exceeding it by an impressive factor of 17.8. The comparison clearly illustrates that sampling-based planners often struggle to efficiently find rule-compliant trajectories. This challenge arises primarily from the discretization of the state space and the design of the cost function [11, (4) and (12)], which does not inherently prioritize rule adherence. In contrast, the runtime of our trajectory repair approach is minimally affected by the cost function selection. Additionally, the sampling-based

¹¹The code base is obtained from <https://commonroad.in.tum.de/tools/commonroad-reactive-planner>.

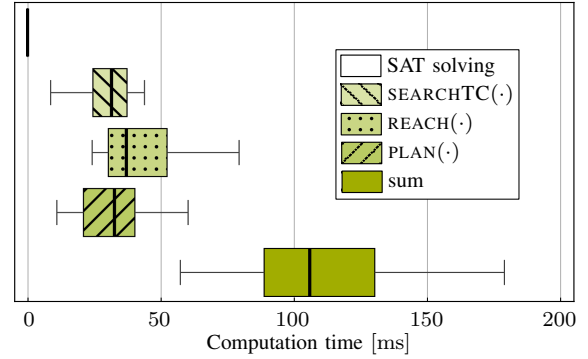


Fig. 12: Benchmarked computation times of our approach, accounting for the total runtime across all iterations within the SMT solver. Outliers are excluded from the box plot for improved clarity.

approach is only resolution- or probabilistically complete, meaning it cannot determine if a rule-compliant trajectory exists or is unattainable – a limitation effectively addressed by our approach.

E. Computation Time

We further illustrate the computation times of components in our trajectory repair approach across the benchmarked 150 dataset scenarios in Fig. 12. The total mean computation time is 114.2ms, with over 96% of cases staying below 200ms, underscoring its real-time capability. The functions $\text{SEARCHTC}(\cdot)$ and $\text{REACH}(\cdot)$ account for the majority of the time, with mean values of 37.5ms and 43.4ms, respectively. Meanwhile, the SAT solving takes an average of 30 μ s. This demonstrates that, even for complex rules in critical urban scenarios, our approach maintains stable and efficient performance across all components. To optimize runtime performance, the codebase could be fully implemented in C++; however, the current performance is already sufficient for our test environment.

To highlight the effectiveness of reachability analysis in reducing computation time during critical situations, we compare the runtime performance of the benchmark scenarios between our approach and the sampling-based planner (cf. Sec. VII-D2), using time-to-collision (TTC) [85] as the criticality measure. The stop line rule is excluded from this comparison because, unlike TTC, it does not involve interactions with other obstacles. The results in Fig. 13 with linear regression demonstrate that the computation time for

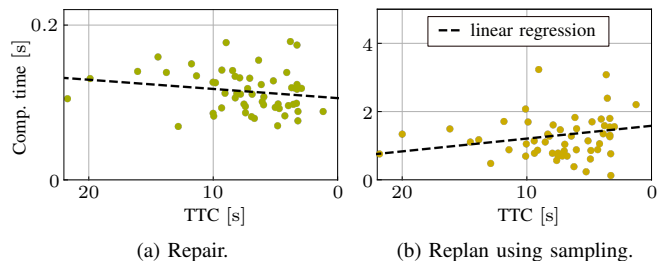
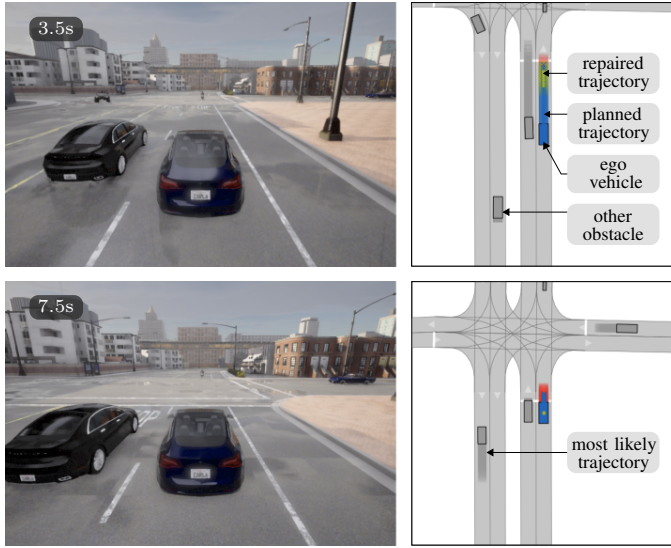
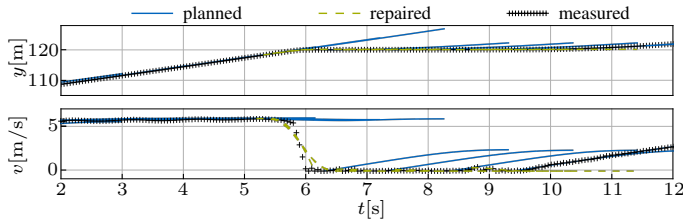


Fig. 13: Relation between the computation time and the TTC. For better insight, the horizontal axis indicates an increase in criticality.



(a) CARLA and CommonRoad scenarios at two time steps.



(b) Nominal and measurement data.

Fig. 14: Repair of the stop line rule, where the ego vehicle successfully waits in front of the stop line for 3s. (a) shows wide-angle snapshots from the CARLA simulator focusing on the ego vehicle, with the CommonRoad scenarios visualized in a bird’s-eye view on the right-hand side. (b) presents selected experimental data, where y denotes the vertical Cartesian position.

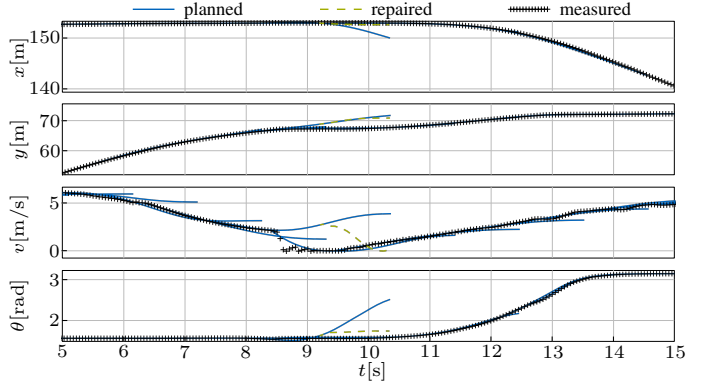
our approach decreases as TTC decreases, indicating improved performance in more challenging scenarios. In contrast, the computation time for the sampling-based planner increases as the scenarios become more critical.

F. CARLA Simulation

We now integrate the proposed trajectory repair approach into the CARLA simulator [101], employing the planning algorithm described in [7] as the nominal planner. The prediction module utilizes a constant acceleration model to forecast the future trajectories of surrounding traffic participants. Specifically, the planning algorithm combines a decision module based on reachability analysis with the solution of an optimal control problem to generate feasible trajectories. However, it explicitly accounts for only a limited subset of traffic rules, such as speed limits and traffic lights. For our experiments, we use the urban downtown environment with CARLA map ID Town 03 and configure the traffic manager in autopilot mode to simulate realistic urban traffic scenarios. The planned trajectories are continuously monitored against formalized urban traffic rules [19] and are repaired by our approach whenever a violation occurs. To address discrepancies between the high-fidelity vehicle model in CARLA and the simplified vehicle models used in both the nominal planner and our repair



(a) CARLA and CommonRoad scenarios at the repair time step.



(b) Nominal and measurement data.

Fig. 15: Repair of the left-turn rule, where the ego vehicle successfully yields to another obstacle inside the intersection. (a) shows a snapshot from the CARLA simulator and CommonRoad scenario, with legends matching those in Fig. 14. (b) presents experimental data for the ego vehicle, where x is the horizontal Cartesian position, and θ is the orientation.

approach, we incorporate a feedback controller to compensate for model uncertainties and disturbances.

Fig. 14 and Fig. 15 display the repair results in the CARLA simulator for the stop line rule φ_{IN1} (cf. Sec. VII-C1) and the left-turn rule φ_{IN5} , respectively. The latter rule restricts the ego vehicle from making a left turn without priority unless it can safely enter the oncoming lane without posing a risk to approaching vehicles. For a detailed formalization of φ_{IN5} , we refer readers to [19, Tab. VI]. Without requiring any tuning of the nominal planner, we adapt the planned trajectory to a rule-compliant solution space through consecutive trajectory repair, even when the nominal planner consistently tends to violate the rule (cf. Fig. 14b). These results highlight the robustness of our approach in a closed-loop environment, emphasizing its readiness for real-world deployment.

G. Real-World Vehicle Deployment

We integrate our approach into the EDGAR research vehicle [102], a Volkswagen T7 Multivan equipped with the necessary sensors and hardware for fully autonomous test runs. Fig. 16 illustrates the real-world test urban scenario, showcasing a stop line in the driveway of the ego vehicle. The repair algorithm is incorporated via the Autoware Universe middleware software stack [103], with the nominal planner provided by the CommonRoad-Autoware interface toolbox [104], which does not explicitly account for any formalized traffic rules. Trajectories generated by the repairer, if they violate a rule, or the nominal planner, if they do not, are then communicated to

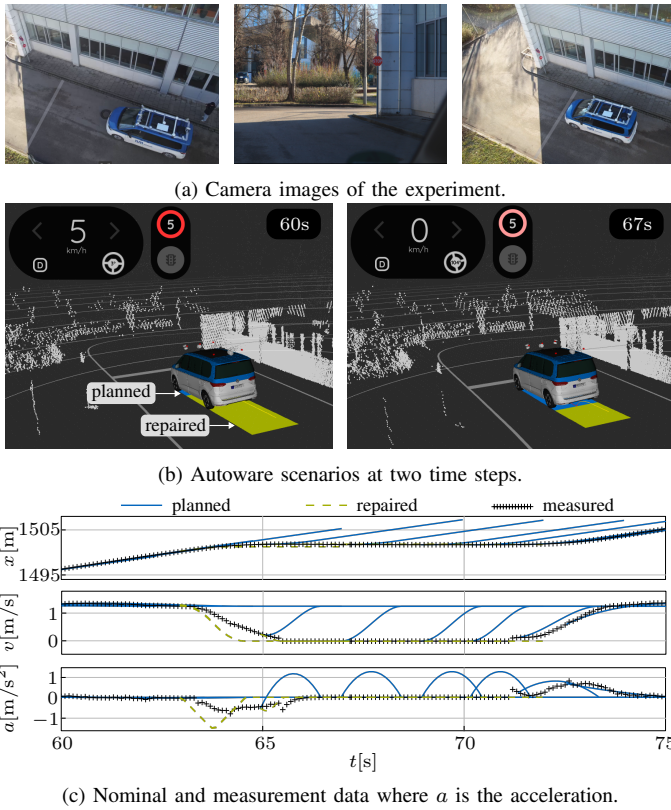


Fig. 16: Situation from our real-world experiments where the nominal planner for the ego vehicle neglects the stop line rule, with its trajectory continuously monitored and effectively repaired by our approach.

the controller through ROS2 [105]. This setup allows the repair approach to operate within the same software environment as previous experiments. As shown in Fig. 16c, through the application of our repair algorithm, the ego vehicle stops precisely in front of the marked stop line for approximately 5s. The duration exceeds the required 3s (cf. Tab. III) due to the heavy computational load of the sensor components, which slows down the planning-monitoring-repair pipeline. While reducing t_{slw} in the rule formula (cf. (4)) or optimizing the entire software stack could mitigate this issue, these aspects are beyond the scope of our work. Additionally, we observe similar driving behavior in the real-world deployment and the CARLA simulator, with differences primarily in the robustness of the controller (cf. Fig. 14b and Fig. 16c). Therefore, we can rely on CARLA for further development before deploying the repair algorithm in real-world scenarios.

VIII. CONCLUSIONS

To the best of our knowledge, we present the first trajectory repair framework for automated vehicles designed to ensure compliance with any formalized traffic rules, provided a feasible solution exists. Our approach modularizes rule formulas and leverages satisfiability modulo theories to determine repair strategies, while reachability analysis prunes the search space after branching from the initial trajectory, enhancing computational efficiency. Although incorporating if-else conditions into the planning module can manage specific traffic rules, they become impractical for comprehensive compliance across all

traffic situations. Our adaptive repair mechanism, independent of the nominal planner, systematically rectifies rule-violating trajectories, similar to how public monitoring systems detect and address violations to uphold order on roads. Through comparisons with state-of-the-art methods and extensive experiments in challenging rules and real-world conditions, we believe our approach marks a significant advancement in enhancing safety and fostering public trust in automated driving.

ACKNOWLEDGMENT

The authors gratefully acknowledge the financial support provided by the German Research Foundation (DFG) under grants AL 1185/7-1 and AL 1185/20-1. The authors also extend their gratitude to the EDGAR team for the complete development of the vehicle and their valuable support during the driving experiments. Special thanks go to M. Wetzlinger for his insightful feedback on earlier drafts of this article and to A. Li for conducting the drone filming for the experiments.

REFERENCES

- [1] D. Gonzalez Bautista, J. Pérez, V. Milanes, and F. Nashashibi, "A review of motion planning techniques for automated vehicles," *IEEE Trans. on Intell. Transp. Systems*, vol. 17, no. 4, pp. 1135–1145, 2015.
- [2] B. Paden, M. Čáp, S. Z. Yong, D. Yershov, and E. Frazzoli, "A survey of motion planning and control techniques for self-driving urban vehicles," *IEEE Trans. on Intell. Vehicles*, vol. 1, no. 1, pp. 33–55, 2016.
- [3] L. Claussmann, M. Revilloud, D. Gruyer, and S. Glaser, "A review of motion planning for highway autonomous driving," *IEEE Trans. on Intell. Transp. Systems*, vol. 21, no. 5, pp. 1826–1848, 2019.
- [4] N. Mehdipour, M. Althoff, R. D. Tebbens, and C. Belta, "Formal methods to comply with rules of the road in autonomous driving: State of the art and grand challenges," *Automatica*, vol. 152, no. 110692, 2023.
- [5] Y. Huang and Y. Chen, "Survey of state-of-art autonomous driving technologies with deep learning," in *Proc. of the IEEE Int. Conf. on Software Quality, Reliability and Security Companion*, 2020, pp. 221–228.
- [6] W. Xiao, N. Mehdipour, A. Collin, A. Y. Bin-Nun, E. Frazzoli, R. D. Tebbens, and C. Belta, "Rule-based optimal control for autonomous driving," in *Proc. of the ACM/IEEE Int. Conf. on Cyber-Physical Systems*, 2021, pp. 143–154.
- [7] N. Kochdumper and S. Bak, "Real-time capable decision making for autonomous driving using reachable sets," in *Proc. of the IEEE Int. Conf. on Robotics and Automation*, 2024, pp. 14 169–14 176.
- [8] A. Rizaldi, J. Keinholz, M. Huber, J. Feldle, F. Immler, M. Althoff, E. Hilgendorf, and T. Nipkow, "Formalising and monitoring traffic rules for autonomous vehicles in Isabelle/HOL," in *Proc. of the Int. Conf. of Integrated Formal Methods*, 2017, pp. 50–66.
- [9] P. Du, Z. Huang, T. Liu, T. Ji, K. Xu, Q. Gao, H. Sibai, K. Driggs-Campbell, and S. Mitra, "Online monitoring for safe pedestrian-vehicle interactions," in *Proc. of the IEEE Int. Conf. on Intell. Transp. Syst.*, 2020, pp. 1–8.
- [10] Y. E. Sahin, R. Quirynen, and S. D. Cairano, "Autonomous vehicle decision-making and monitoring based on signal temporal logic and mixed-integer programming," in *Proc. of the American Control Conf.*, 2020, pp. 454–459.
- [11] M. Werling, S. Kammel, J. Ziegler, and L. Gröll, "Optimal trajectories for time-critical street scenarios using discretized terminal manifolds," *The Int. Journal of Robotics Research*, vol. 31, no. 3, pp. 346–359, 2012.
- [12] G. E. Fainekos, "Revising temporal logic specifications for motion planning," in *Proc. of the IEEE Int. Conf. on Robotics and Automation*, 2011, pp. 40–45.
- [13] R. Alur, S. Moarref, and U. Topcu, "Counter-strategy guided refinement of GR(1) temporal logic specifications," in *Proc. of the Formal Methods in Computer-Aided Design*, 2013, pp. 26–33.
- [14] A. Pacheck and H. Kress-Gazit, "Physically feasible repair of reactive, linear temporal logic-based, high-level tasks," *IEEE Trans. on Robotics*, vol. 39, no. 6, pp. 4653–4670, 2023.

- [15] A. Rizaldi, F. Immler, B. Schürmann, and M. Althoff, "A formally verified motion planner for autonomous vehicles," in *Proc. of the Int. Symposium on Automated Technology for Verification and Analysis*, 2018, pp. 75–90.
- [16] K. Esterle, L. Gressenbuch, and A. Knoll, "Formalizing traffic rules for machine interpretability," in *Proc. of the IEEE Connected and Automated Vehicles Symp.*, 2020, pp. 1–7.
- [17] S. Maierhofer, A.-K. Rettinger, E. C. Mayer, and M. Althoff, "Formalization of interstate traffic rules in temporal logic," in *Proc. of the IEEE Intell. Vehicles Symp.*, 2020, pp. 752–759.
- [18] H. Krasowski and M. Althoff, "Temporal logic formalization of marine traffic rules," in *Proc. of the IEEE Intell. Vehicles Symp.*, 2021, pp. 186–192.
- [19] S. Maierhofer, P. Moosbrugger, and M. Althoff, "Formalization of intersection traffic rules in temporal logic," in *Proc. of the IEEE Intell. Vehicles Symp.*, 2022, pp. 1135–1144.
- [20] N. Aréchiga, "Specifying safety of autonomous vehicles in signal temporal logic," in *Proc. of the IEEE Intell. Veh. Symp.*, 2019, pp. 58–63.
- [21] C.-I. Vasile, J. Tumova, S. Karaman, C. Belta, and D. Rus, "Minimum-violation sLTL motion planning for mobility-on-demand," in *Proc. of the IEEE Int. Conf. on Robotics and Automation*, 2017, pp. 1481–1488.
- [22] A. Dokhanchi, H. B. Amor, J. V. Deshmukh, and G. Faïnekos, "Evaluating perception systems for autonomous vehicles using quality temporal logic," in *Runtime Verification*, vol. 11237, 2018, pp. 409–416.
- [23] S. M. LaValle and J. J. Kuffner, "Rapidly-exploring random trees: Progress and prospects," *Algorithmic and Computational Robotics: New Directions*, vol. 5, pp. 293–308, 2001.
- [24] L. I. R. Castro, P. Chaudhari, J. Tumová, S. Karaman, E. Frazzoli, and D. Rus, "Incremental sampling-based algorithm for minimum-violation motion planning," in *Proc. of the IEEE Conf. on Decision and Control*, 2013, pp. 3217–3224.
- [25] F. S. Barbosa, L. Lindemann, D. V. Dimarogonas, and J. Tumova, "Integrated motion planning and control under metric interval temporal logic specifications," in *Proc. of the IEEE European Control Conf.*, 2019, pp. 2042–2049.
- [26] C. I. Vasile, X. Li, and C. Belta, "Reactive sampling-based path planning with temporal logic specifications," *The Int. Journal of Robotics Research*, vol. 39, no. 8, pp. 1002–1028, 2020.
- [27] S. Karaman and E. Frazzoli, "Incremental sampling-based algorithms for optimal motion planning," *Proc. of Robotics: Science and Systems*, vol. 104, no. 2, pp. 267–274, 2010.
- [28] G. E. Faïnekos and G. J. Pappas, "Robustness of temporal logic specifications for continuous-time signals," *Theoretical Computer Science*, vol. 410, no. 42, pp. 4262–4291, 2009.
- [29] A. Donzé and O. Maler, "Robust satisfaction of temporal logic over real-valued signals," in *Proc. of the Int. Conf. on Formal Modeling and Analysis of Timed Systems*, 2010, pp. 92–106.
- [30] C. Belta and S. Sadraddini, "Formal methods for control synthesis: An optimization perspective," *Annual Review of Control, Robotics, and Autonomous Systems*, vol. 2, pp. 115–140, 2019.
- [31] L. Lindemann and D. V. Dimarogonas, "Control barrier functions for signal temporal logic tasks," *IEEE Control Systems Letters*, vol. 3, no. 1, pp. 96–101, 2018.
- [32] W. Liu, N. Mehdipour, and C. Belta, "Recurrent neural network controllers for signal temporal logic specifications subject to safety constraints," *IEEE Control Systems Letters*, vol. 6, pp. 91–96, 2021.
- [33] K. Leung, N. Aréchiga, and M. Pavone, "Backpropagation through signal temporal logic specifications: Infusing logical structure into gradient-based methods," *The Int. Journal of Robotics Research*, vol. 42, no. 6, pp. 356–370, 2023.
- [34] E. Irani Liu and M. Althoff, "Computing specification-compliant reachable sets for motion planning of automated vehicles," in *Proc. of the IEEE Intell. Vehicles Symp.*, 2021, pp. 1–8.
- [35] —, "Specification-compliant driving corridors for motion planning of automated vehicles," *IEEE Trans. on Intell. Vehicles*, vol. 8, no. 9, pp. 4180–4197, 2023.
- [36] F. Lercher and M. Althoff, "Specification-compliant reachability analysis for autonomous vehicles using on-the-fly model checking," in *Proc. of the IEEE Intell. Vehicles Symp.*, 2024, pp. 1484–1491.
- [37] S. Koenig and M. Likhachev, "Incremental A*," *Proc. of the Advances in Neural Information Processing Systems*, vol. 14, 2001.
- [38] S. Koenig, M. Likhachev, and D. Furcy, "Lifelong planning A*," *Artificial Intell.*, vol. 155, no. 1-2, pp. 93–146, 2004.
- [39] A. Stentz and I. C. Mellon, "Optimal and efficient path planning for unknown and dynamic environments," *Int. Journal of Robotics and Automation*, vol. 10, no. 3, pp. 89–100, 1995.
- [40] M. Likhachev, G. J. Gordon, and S. Thrun, "ARA*: Anytime A* with provable bounds on sub-optimality," *Proc. of the Advances in Neural Information Processing Systems*, vol. 16, 2003.
- [41] D. Ferguson, N. Kalra, and A. Stentz, "Replanning with RRTs," in *Proc. of the IEEE Int. Conf. on Robotics and Automation*, 2006, pp. 1243–1248.
- [42] S. Karaman, M. R. Walter, A. Perez, E. Frazzoli, and S. Teller, "Anytime motion planning using the RRT*," in *Proc. of the IEEE Int. Conf. on Robotics and Automation*, 2011, pp. 1478–1483.
- [43] M. Otte and E. Frazzoli, "RRT*: Real-time motion planning/replanning for environments with unpredictable obstacles," in *Algorithmic Foundations of Robotics XI*, vol. 107, 2015, pp. 461–478.
- [44] D. Connell and H. M. La, "Dynamic path planning and replanning for mobile robots using RRT*," in *Proc. of the IEEE Int. Conf. on Systems, Man, and Cybernetics*, 2017, pp. 1429–1434.
- [45] B. Chandler and M. A. Goodrich, "Online RRT* and online FMT*: Rapid replanning with dynamic cost," in *Proc. of the IEEE/RSJ Int. Conf. on Intell. Robots and Systems*, 2017, pp. 6313–6318.
- [46] M. Guo, K. H. Johansson, and D. V. Dimarogonas, "Revising motion planning under linear temporal logic specifications in partially known workspaces," in *Proc. of the IEEE Int. Conf. on Robotics and Automation*, 2013, pp. 5025–5032.
- [47] M. Guo and D. V. Dimarogonas, "Multi-agent plan reconfiguration under local LTL specifications," *The Int. Journal of Robotics Research*, vol. 34, no. 2, pp. 218–235, 2015.
- [48] M. Lahijanian, M. R. Maly, D. Fried, L. E. Kavraki, H. Kress-Gazit, and M. Y. Vardi, "Iterative temporal planning in uncertain environments with partial satisfaction guarantees," *IEEE Trans. on Robotics*, vol. 32, no. 3, pp. 583–599, 2016.
- [49] Y. S. Shao, C. Chen, S. Kousik, and R. Vasudevan, "Reachability-based trajectory safeguard (RTS): A safe and fast reinforcement learning safety layer for continuous control," *IEEE Robotics and Automation Letters*, vol. 6, no. 2, pp. 3663–3670, 2021.
- [50] J. Lin, W. Zhou, H. Wang, Z. Cao, W. Yu, C. Zhao, D. Zhao, D. Yang, and J. Li, "Road traffic law adaptive decision-making for self-driving vehicles," in *Proc. of the IEEE Int. Intell. Transp. Systems Conf.*, 2022, pp. 2034–2041.
- [51] Y. Lin, C. Li, M. Ding, M. Tomizuka, W. Zhan, and M. Althoff, "DrPlanner: Diagnosis and repair of motion planners for automated vehicles using large language models," *IEEE Robotics and Automation Letters*, vol. 9, no. 10, pp. 8218–8225, 2024.
- [52] M. Kalakrishnan, S. Chitta, E. Theodorou, P. Pastor, and S. Schaal, "STOMP: Stochastic trajectory optimization for motion planning," in *Proc. of the Int. Conf. on Robotics and Automation*, 2011, pp. 4569–4574.
- [53] B. Lau, C. Sprunk, and W. Burgard, "Kinodynamic motion planning for mobile robots using splines," in *Proc. of the IEEE/RSJ Int. Conf. on Intell. Robots and Systems*, 2009, pp. 2427–2433.
- [54] M. Phillips and M. Likhachev, "SIPP: Safe interval path planning for dynamic environments," in *Proc. of the IEEE Int. Conf. on Robotics and Automation*, 2011, pp. 5628–5635.
- [55] M. Zucker, N. Ratliff, A. D. Dragan, M. Pivtoraiko, M. Klingensmith, C. M. Dellin, J. A. Bagnell, and S. S. Srinivasa, "CHOMP: Covariant Hamiltonian optimization for motion planning," *The Int. Journal of robotics research*, vol. 32, no. 9-10, pp. 1164–1193, 2013.
- [56] V. Usenko, L. von Stumberg, A. Pangercic, and D. Cremers, "Real-time trajectory replanning for MAVs using uniform B-splines and a 3D circular buffer," in *Proc. of the IEEE/RSJ Int. Conf. on Intell. Robots and Systems*, 2017, pp. 215–222.
- [57] S. Liu, M. Watterson, K. Mohta, K. Sun, S. Bhattacharya, C. J. Taylor, and V. Kumar, "Planning dynamically feasible trajectories for quadrotors using safe flight corridors in 3-D complex environments," *IEEE Robotics and Automation Letters*, vol. 2, no. 3, pp. 1688–1695, 2017.
- [58] W. Ding, W. Gao, K. Wang, and S. Shen, "Trajectory replanning for quadrotors using kinodynamic search and elastic optimization," in *Proc. of the IEEE Int. Conf. on Robotics and Automation*, 2018, pp. 7595–7602.
- [59] M. Missura, A. Roychoudhury, and M. Bennewitz, "Fast-replanning motion control for non-holonomic vehicles with aborting A*," in *Proc. of the IEEE/RSJ Int. Conf. on Intell. Robots and Systems*, 2022, pp. 10267–10274.

- [60] C. Roesmann, W. Feiten, T. Woesch, F. Hoffmann, and T. Bertram, "Trajectory modification considering dynamic constraints of autonomous robots," in *Proc. of the German Conf. on Robotics*, 2012, pp. 1–6.
- [61] Q.-C. Pham, "Fast trajectory correction for nonholonomic mobile robots using affine transformations," *Proc. of Robotics: Science and Systems*, pp. 265–272, 2012.
- [62] J. Ziegler, P. Bender, T. Dang, and C. Stiller, "Trajectory planning for Bertha—a local, continuous method," in *Proc. of the IEEE Intell. Vehicles Symp.*, 2014, pp. 450–457.
- [63] W. Ding, L. Zhang, J. Chen, and S. Shen, "Epsilon: An efficient planning system for automated vehicles in highly interactive environments," *IEEE Trans. on Robotics*, vol. 38, no. 2, pp. 1118–1138, 2021.
- [64] Y. Chen, U. Rosolia, W. Ubellacker, N. Csomay-Shanklin, and A. D. Ames, "Interactive multi-modal motion planning with branch model predictive control," *IEEE Robotics and Automation Letters*, vol. 7, no. 2, pp. 5365–5372, 2022.
- [65] R. Wang, M. Schuurmans, and P. Patrinos, "Interaction-aware model predictive control for autonomous driving," in *Proc. of the IEEE European Control Conf.*, 2023, pp. 1–6.
- [66] T. Li, L. Zhang, S. Liu, and S. Shen, "MARC: Multipolicy and risk-aware contingency planning for autonomous driving," *IEEE Robotics and Automation Letters*, vol. 8, no. 10, pp. 6587–6594, 2023.
- [67] K. Tong, S. Solmaz, M. Horn, M. Stolz, and D. Watznig, "Robust tunable trajectory repairing for autonomous vehicles using Bernstein basis polynomials and path-speed decoupling," in *Proc. of the IEEE Int. Intell. Transp. Systems Conf.*, 2023, pp. 8–15.
- [68] L. Peters, A. Bajcsy, C.-Y. Chiu, D. Fridovich-Keil, F. Laine, L. Ferranti, and J. Alonso-Mora, "Contingency games for multi-agent interaction," *IEEE Robotics and Automation Letters*, vol. 9, no. 3, pp. 2208–2215, 2024.
- [69] C. Pek and M. Althoff, "Fail-safe motion planning for online verification of autonomous vehicles using convex optimization," *IEEE Trans. on Robotics*, vol. 37, no. 3, pp. 798–814, 2021.
- [70] Y. Lin, S. Maierhofer, and M. Althoff, "Sampling-based trajectory repairing for autonomous vehicles," in *Proc. of the IEEE Int. Intell. Transp. Systems Conf.*, 2021, pp. 572–579.
- [71] Y. Wang, Y. Lin, and M. Althoff, "Interaction-aware trajectory repair in compliance with formalized traffic rules," in *Proc. of the IEEE Int. Intell. Transp. Systems Conf.*, 2024.
- [72] Y. Lin and M. Althoff, "Rule-compliant trajectory repairing using satisfiability modulo theories," in *Proc. of the IEEE Intell. Vehicles Symp.*, 2022, pp. 449–456.
- [73] C. Barrett and C. Tinelli, "Satisfiability modulo theories," in *Handbook of Model Checking*, 2018, pp. 305–343.
- [74] P. Bender, J. Ziegler, and C. Stiller, "Lanelets: Efficient map representation for autonomous driving," in *Proc. of the IEEE Intell. Vehicles Symp.*, 2014, pp. 420–425.
- [75] G. Würsching and M. Althoff, "Robust and efficient curvilinear coordinate transformation with guaranteed map coverage for motion planning," in *Proc. of the IEEE Intell. Vehicles Symp.*, 2024, pp. 2694–2701.
- [76] E. Bartocci, J. Deshmukh, A. Donzé, G. Fainekos, O. Maler, D. Ničković, and S. Sankaranarayanan, "Specification-based monitoring of cyber-physical systems: A survey on theory, tools and applications," in *Lectures on Runtime Verification*, 2018, pp. 135–175.
- [77] S. Sadraddini and C. Belta, "Robust temporal logic model predictive control," in *Proc. of the Annual Allerton Conf. on Communication, Control, and Computing*, 2015, pp. 772–779.
- [78] R. Sebastiani, "Lazy satisfiability modulo theories," *Journal on Satisfiability, Boolean Modeling and Computation*, vol. 3, no. 3-4, pp. 141–224, 2007.
- [79] P. Halder and M. Althoff, "Minimum-violation velocity planning with temporal logic constraints," in *Proc. of the IEEE Int. Intell. Transp. Systems Conf.*, 2022, pp. 2520–2527.
- [80] J. S. Warford, D. Vega, and S. M. Staley, "A calculational deductive system for linear temporal logic," *ACM Computing Surveys*, vol. 53, no. 3, pp. 1–38, 2020.
- [81] Z. Zhang and S. Haesaert, "Modularized control synthesis for complex signal temporal logic specifications," in *Proc. of the IEEE Conf. on Decision and Control*, 2023, pp. 7856–7861.
- [82] G. S. Tseitin, "On the complexity of derivation in propositional calculus," in *Automation of Reasoning*, 1983, pp. 466–483.
- [83] M. Davis, G. Logemann, and D. Loveland, "A machine program for theorem-proving," *Communications of the ACM*, vol. 5, no. 7, pp. 394–397, 1962.
- [84] Y. Lin, H. Li, and M. Althoff, "Model predictive robustness of signal temporal logic predicates," *IEEE Robotics and Automation Letters*, vol. 08, no. 12, pp. 8050–8057, 2023.
- [85] Y. Lin and M. Althoff, "CommonRoad-CriMe: A toolbox for criticality measures of autonomous vehicles," in *Proc. of the IEEE Intell. Veh. Symp.*, 2023, pp. 1–8.
- [86] H. Krasowski, Y. Zhang, and M. Althoff, "Safe reinforcement learning for urban driving using invariably safe braking sets," in *Proc. of the IEEE Int. Intell. Transp. Systems Conf.*, 2022, pp. 2407–2414.
- [87] R. Nieuwenhuis, A. Oliveras, and C. Tinelli, "Solving SAT and SAT modulo theories: From an abstract Davis–Putnam–Logemann–Loveland procedure to DPLL(T)," *Journal of the ACM*, vol. 53, no. 6, pp. 937–977, 2006.
- [88] A. Tamke, T. Dang, and G. Breuel, "A flexible method for criticality assessment in driver assistance systems," in *Proc. of the IEEE Intell. Vehicles Symposium*, 2011, pp. 697–702.
- [89] S. Boyd and L. Vandenberghe, *Convex Optimization*. Cambridge: Cambridge University Press, 2004.
- [90] S. Manzinger, C. Pek, and M. Althoff, "Using reachable sets for trajectory planning of automated vehicles," *IEEE Trans. on Intell. Vehicles*, vol. 6, no. 2, pp. 232–248, 2020.
- [91] J. Gardner, G. Pleiss, K. Q. Weinberger, D. Bindel, and A. G. Wilson, "GPY Torch: Blackbox matrix-matrix Gaussian process inference with GPU acceleration," in *Proc. of the Conf. on Neural Information Processing Syst.*, 2018, pp. 7576–7586.
- [92] T. Yamaguchi, B. Hoxha, and D. Ničković, "RTAMT—runtime robustness monitors with application to CPS and robotics," *Int. Journal on Software Tools for Technology Transfer*, vol. 26, no. 1, pp. 79–99, 2024.
- [93] E. Irani Liu, G. Würsching, M. Klischat, and M. Althoff, "CommonRoad-Reach: A toolbox for reachability analysis of automated vehicles," in *Proc. of the IEEE Int. Intell. Transp. Systems Conf.*, 2022, pp. 2313–2320.
- [94] Gurobi Optimization, LLC, "Gurobi Optimizer Reference Manual," 2024. [Online]. Available: <https://www.gurobi.com>
- [95] R. Krajewski, J. Bock, L. Kloecker, and L. Eckstein, "The highD dataset: A drone dataset of naturalistic vehicle trajectories on German highways for validation of highly automated driving systems," in *Proc. of the IEEE Int. Intell. Transp. Systems Conf.*, 2018, pp. 2118–2125.
- [96] J. Bock, R. Krajewski, T. Moers, S. Runde, L. Vater, and L. Eckstein, "The inD dataset: A drone dataset of naturalistic road user trajectories at German intersections," in *Proc. of the IEEE Intell. Vehicles Symp.*, 2020, pp. 1929–1934.
- [97] M. Althoff, M. Koschi, and S. Manzinger, "CommonRoad: Composable benchmarks for motion planning on roads," in *Proc. of the IEEE Intell. Vehicles Symp.*, 2017, pp. 719–726.
- [98] V. Raman, M. Maasoumy, and A. Donzé, "Model predictive control from signal temporal logic specifications: A case study," in *Proc. of the ACM SIGBED Int. Workshop on Design, Modeling, and Evaluation of Cyber-Physical Systems*, 2014, pp. 52–55.
- [99] V. Kurtz and H. Lin, "Mixed-integer programming for signal temporal logic with fewer binary variables," *IEEE Control Systems Letters*, vol. 6, pp. 2635–2640, 2022.
- [100] P. Halder, F. Christ, and M. Althoff, "Lexicographic mixed-integer motion planning with STL constraints," in *Proc. of the IEEE Int. Intell. Transp. Systems Conf.*, 2023, pp. 2034–2041.
- [101] A. Dosovitskiy, G. Ros, F. Codevilla, A. Lopez, and V. Koltun, "CARLA: An open urban driving simulator," in *Proc. of the Conf. on Robot Learning*, 2017, pp. 1–16.
- [102] P. Karle, T. Betz, M. Bosk, F. Fent, N. Gehrke, M. Geisslinger, L. Gressenbuch, P. Hafemann, S. Huber, M. Hübner, et al., "EDGAR: An autonomous driving research platform – from feature development to real-world application," *arXiv preprint arXiv:2309.15492*, 2024.
- [103] S. Kato, S. Tokunaga, Y. Maruyama, S. Maeda, M. Hirabayashi, Y. Kitsukawa, A. Monroy, T. Ando, Y. Fujii, and T. Azumi, "Autoware on board: Enabling autonomous vehicles with embedded systems," in *Proc. of the ACM/IEEE Int. Conf. on Cyber-Physical Systems*, 2018, pp. 287–296.
- [104] G. Würsching, T. Mascetta, Y. Lin, and M. Althoff, "Simplifying Sim-to-Real transfer in autonomous driving: Coupling autoware with the CommonRoad motion planning framework," in *Proc. of the IEEE Intell. Vehicles Symp.*, 2024, pp. 1462–1469.
- [105] S. Macenski, T. Foote, B. Gerkey, C. Lalancette, and W. Woodall, "Robot operating system 2: Design, architecture, and uses in the wild," *Science robotics*, vol. 7, no. 66, pp. 1–10, 2022.

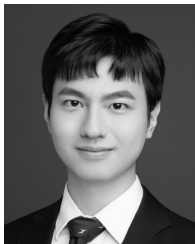


Yuanfei Lin is currently a Ph.D. candidate in the Cyber-Physical Systems Group at the Technical University of Munich, Germany, under the supervision of Prof. Dr.-Ing. Matthias Althoff. He received his B.Eng. degree in Automotive Engineering from Tongji University, China, in 2018, and dual M.Sc. degrees in Mechanical Engineering and Mechatronics and Robotics at the Technical University of Munich, Germany, in 2020. In 2023, he was a visiting scholar at the University of California, Berkeley, USA. His research interests include motion planning

for automated vehicles, formal methods, and the application of large language models.



Zekun Xing is currently a Ph.D. student in the Chair of Automatic Control Engineering at the Technical University of Munich, Germany. He received his B.Eng. degree in Automotive Engineering and Service from Tongji University, China, in 2021, and M.Sc. degree in Mechatronics and Robotics at the Technical University of Munich, Germany, in 2023. His research interests include motion prediction and planning for autonomous vehicles, decision-making in interactive driving scenarios, and model predictive control with application in automated driving.



Xuyuan Han is currently pursuing his M.Sc. degree in Robotics, Cognition, Intelligence at the Technical University of Munich, Germany. He received his B.Eng. degree in Mechatronics from Tongji University, China, in 2022. His research interests include motion planning for autonomous vehicles and the integration of vision-language models in end-to-end autonomous driving systems.



Matthias Althoff is an associate professor in computer science at the Technical University of Munich, Germany. He received his diploma engineering degree in Mechanical Engineering in 2005, and his Ph.D. degree in Electrical Engineering in 2010, both from the Technical University of Munich, Germany. From 2010 to 2012 he was a postdoctoral researcher at Carnegie Mellon University, Pittsburgh, USA, and from 2012 to 2013 an assistant professor at Technische Universität Ilmenau, Germany. His research interests include formal verification of continuous

and hybrid systems, reachability analysis, planning algorithms, nonlinear control, automated vehicles, and power systems.